SSRG International Journal of Civil Engineering
ISSN: 2348-8352/ https://doi.org/10.14445/23488352/IJCE-V13I8P131

Volume 13 Issue 8, 526-559, August 2026

Original Article

Microstructure-Driven Strength and Durability Optimization of Structural Concrete Incorporating Iron Ore Tailings

Om V.Vaidya[1], Urmila R. Kawade[2], Nagashree[3], Nita Mehta[4], Vinayak A Hosur[5], Rakh Avinash Angadrao[6], Prashant Sunagar[7]

[1]*Dept of Civil engineering, SNJB's Late Sau. Kantabai Bhavarlalji Jain College of Engineering, Chandwad, Maharashtra, India.*
[2]*Department of Civil Engineering, Dr.V.V.Patil COE, Ahilyanagar. Maharashtra, India.*
[3]*Department of Civil Engineering, M S Ramaiah Institute of Technology, Bangalore, India.*
[4]*Department of Chemical Engineering, Thadomal Shahani Engineering College Mumbai, India.*
[5]*Department of Civil Engineering, Dayananda Sagar Academy of Technology and Management, Bangalore, India.*
[6]*Department of Civil Engineering, MIT School of Engineering & Sciences, MITADT University, Pune, India.*
[7]*Department of Civil Engineering, Sandip Institute of Technology and Research, Nashik, Maharashtra, India.*

[7]*Corresponding Author : prashant.sjce@gmail.com*

Received: 26 March 2026 Revised: 01 June 2026 Accepted: 12 August 2026 Published: 31 August 2026

Abstract *- Unsustainable extraction of river sand has caused widespread ecological damage and created an urgent need for alternative fine aggregates. Iron Ore Tailings (IOT), generated in bulk during iron ore beneficiation and presently managed by stockpiling, constitute a candidate waste stream for valorisation in cementitious systems. This study evaluates IOT as a replacement for manufactured sand in mortar and structural concrete using a hierarchical mortar-to-concrete optimisation framework. Cement mortars were produced at IOT replacement levels of 0 to 100 per cent and water-cement ratios of 0.40, 0.50 and 0.60 at a 1:3 binder-to-aggregate ratio, and the optimum identified at mortar scale was transferred to M25 concrete cast at water-cement ratios of 0.50 and 0.60. Replacement of 40 per cent of the manufactured sand raised the 28-day compressive strength from 35.24 to 39.02 MPa at a water-cement ratio of 0.50, a gain of 10.7 per cent that remains statistically significant for any within-triplicate coefficient of variation up to 4.49 per cent. Flexural capacity was preserved rather than improved, and the reductions in splitting tensile strength of 8.4 and 7.6 per cent and in slump of 9.6 and 8.3 per cent, although consistent in direction, lie within the typical precision of those tests at three replicates. Charge passed decreased monotonically from 160 to 144 coulombs across 0 to 60 per cent replacement, all mixes remaining within the very low permeability class of ASTM C1202. A second-order response surface fitted to the mortar means places the stationary point at 27 to 30 per cent, and the optimum is accordingly reported as a range of 30 to 40 per cent rather than as a sharp maximum. The strength gain is attributed to packing densification and capillary void refinement rather than to pozzolanic reaction, an interpretation supported by the low calcium oxide and amorphous contents of the tailings and benchmarked against published pore structure and interfacial transition zone data for comparable IOT concrete. Cradle-to-gate assessment gives a 1.1 per cent reduction in global warming potential per cubic metre, a 10.7 per cent reduction in carbon intensity per megapascal and a 7.6 per cent reduction if the strength margin is reinvested as a binder reduction, with material cost falling 5.4 per cent per cubic metre within a break-even haul distance of about 200 km. IOT is therefore established as a technically competitive and environmentally preferable fine aggregate for structural concrete.*

Keywords *- Iron ore, RCPT, Durability, WRI, Age-dependent Durability, Combined performances.*

1. Introduction

The rapid expansion of infrastructure development has led to explosive consumption of natural building materials, and river sand in particular, whose extraction has become a significant source of ecological damage. The overexploitation of river sand disrupts riverine ecology, increases riverbank erosion, reduces groundwater recharge and water quality, and creates long-term environmental and socio-economic risks. These issues have sparked a concerted effort to identify alternative fine aggregates that are both technically suitable for incorporation into concrete and, ideally, more sustainable and able to contribute to a circular resource economy.

Meanwhile, the global expansion of iron and steel production is creating a rapidly growing waste stream in the form of IOT, a pulverized mineral by-product of the processing of iron ore. With annual iron ore production already exceeding 2 billion tons, the volume of IOT produced has reached unprecedented levels, making it one of the largest industrial waste products in the world. In many regions, including India, IOT is piling up in tailings ponds or landfills; its fine particulate nature creates conflicts over land use and poses potential problems for air, soil, and water pollution. Despite its favourable mineralogical composition, IOT remains underutilised, and the long-term management of its vast stockpiles is becoming a serious issue for the mining industry.

From the materials engineering perspective, IOT has a number of physicochemical properties, including its high silica and iron oxide content, an angular particle morphology, and a fineness modulus range that is similar to that of natural sand, that suggest that IOT can be used as a fine aggregate in cement-based composite materials. The use of IOT as an aggregate in concrete would both relieve pressure on natural sand supplies and help address the waste problem at its source. However, the properties of IOT need to be related to the performance of concrete in order to facilitate its use. Thus, it is of interest to investigate how IOT affects concrete properties and how it affects concrete microstructure development and strength gain.

It is known that industrial by-products can affect the behavior of concrete through various mechanisms, including particle packing optimization, void refinement, and the densification of the ITZ. The effects of IOT on concrete performance, however, have not yet been systematically studied. In particular, previous work on optimizing the use of IOT as a replacement for natural fine aggregates has yielded variable results regarding the identification of an optimal replacement level of IOT for fine aggregate in concrete mortars or mixes. The variation in the results appears to stem from differences in the tailings from which the samples were obtained and differences in the strategies that were employed for the mix design. In this instance, therefore, there is a need for a more systematic and performance-focused approach.

Notwithstanding this body of work, three specific deficiencies persist. First, the reported optimum IOT replacement level spans an unusually wide band of 10 to 60 per cent, largely because most investigations proceed directly to concrete scale without an intermediate, aggregate-dominated screening step that isolates the fine-aggregate contribution from coarse-aggregate grading and air-entrainment effects. Second, the reported strength gains are seldom rationalised quantitatively; matrix densification is invoked qualitatively but is rarely linked to a measured change in capillary porosity or in interfacial transition zone width. Third, mechanical and transport properties are usually reported in isolation, so no single replacement level has been demonstrated to satisfy compressive, tensile, workability and chloride-transport requirements simultaneously. The practical consequence is that a design engineer presently has no defensible basis on which to specify an IOT content for a structural grade of concrete.

The present study addresses these deficiencies through a hierarchical mortar-to-concrete optimisation strategy in which the replacement level is first screened across the full 0 to 100 per cent range at three water-cement ratios in a 1:3 mortar system, and the resulting optimum is subsequently validated in M25 structural concrete. Performance is then normalised through a set of dimensionless efficiency indices so that compressive, tensile, flexural, workability and chloride-transport responses may be compared on a common basis, and the outcome is benchmarked against published IOT, fly ash and ground granulated blast-furnace slag systems in terms of technical performance, delivered cost and environmental burden. The remainder of the paper is organised as follows: Section 2 reviews the literature and states the research gap and novelty; Section 3 describes the materials and mix design; Section 4 sets out the experimental, statistical and microstructural programme; Sections 5 and 6 present the mechanical, microstructural and durability results; Sections 7 to 9 address environmental and economic assessment, data-driven modelling and field implications; and Section 10 concludes.

In this work, the experimental feasibility of using IOT as a partial replacement for natural fine aggregate in mortar and structural concrete is assessed. The approach adopted is hierarchical: an optimised mix design is developed at mortar scale to identify an optimal replacement level for IOT relative to natural fine aggregate, and this design is then evaluated in M25-grade structural concrete. The research focuses on the relationships among IOT content, packing efficiency, capillary pore refinement and the mechanical and transport performance of the resulting concrete. By establishing a rational framework that relates the specific physical properties of IOT to macroscopic performance, the work seeks to provide a defensible basis for the sustainable use of IOT as a structural fine aggregate.

2. Literature Review

IOT are increasingly being investigated as a potential replacement for fine aggregates in concrete in an effort to mitigate the environmental impact of sand mining and waste disposal [5, 10, 11]. The literature regarding IOT-based concrete is extensive and provides information regarding the impact of IOT replacement on the workability, strength, durability, and microstructure of the resulting concrete. The workability of concretes that utilize IOT as an aggregate replacement tends to decrease with the increased inclusion of IOT relative to natural sand-based aggregates; the angular and highly absorbent nature of IOT particles compared to the more rounded and less-absorbent properties of natural sand contributes to the reduction in workability of concretes containing IOT [5, 10, 13]. Furthermore, the workability of concrete with IOT-based aggregates decreases in a linear relationship with the increased dosage of IOT; however, IOT concrete remains workable up to approximately 40-45% IOT replacement of natural sand-based aggregates [5]. IOT-based concretes, however, experience a loss of flowability if natural sand is completely replaced by IOT [1, 6, 18]. Additionally, the strength of concretes with IOT-based aggregates exhibits a non-monotonic trend with increased IOT replacement levels. For conventional concretes, strength increases with IOT replacement levels up to approximately 20-40%, after which strength begins to plateau or even decrease with the increase in IOT dosage [5, 7, 12]. Studies that assessed the compressive strength of IOT-based concretes have found that the strength of those concretes is typically maximized at around 10-30% IOT replacement levels [7, 8, 12, 13].

Other studies, however, have reported that 25-40% IOT levels are typically associated with the maximum strength of concrete with IOT-based aggregates [5, 10, 11]. The impact of IOT on the strength of ultra-high-performance concretes and mortars is similar to that of conventional concretes; concretes with IOT exhibit similar strength levels to concretes with natural sand up to 40% IOT replacement levels, but strength decreases with the complete replacement of natural sand with IOT [6, 18]. Similar results are also present for IOT-based ultra-high-performance concretes and mortars, where concretes with IOT exhibit similar strength levels to natural sand-based concretes and mortars at IOT levels of 20-25% [1, 19]. The reason for these trends is due to two main mechanisms related to the properties of IOT aggregates. First, one potential reason that concretes with IOT exhibit increased strength is due to the effect of the IOT aggregates as micro-aggregates or fillers that help the concrete to densify [1, 4, 8, 15, 18]. Second, some studies suggest that there are additional, chemical-related reasons for the increased strength of concretes with IOT replacement; the crystalline components of IOT are considered to be inert fillers within the concretes, but the amorphous components of the IOT react chemically with the components of cement (calcium hydroxide) to form additional cement-like binding phases [1, 4, 19]. Beyond these reasons for increased strength of concretes with IOT replacement, it is also suggested that increased levels of IOT replacement beyond those that exhibit maximum strength of the concretes lead to the introduction of microcracks into the concretes that act to reduce the strength and integrity of those concretes [1, 8, 18].

Related to these findings regarding the strength of concrete with IOT-based aggregates is the durability of those concretes. Similar to the trend for strength, concretes that include IOT-based aggregates exhibit reduced porosity, water absorption, and chloride permeability if the IOT-based aggregates are included at rates of approximately 20-40% of the total aggregate for the concrete [4, 9, 13, 18, 20]. The use of IOT-based aggregates leads to increased resistance of concretes to the effects of sulfate attack, drying and wetting cycles, and freeze and thaw cycles [3, 20]. Additionally, incorporating calcium carbonate whiskers into IOT-based concrete helps to ensure that the durability of those concretes is maintained even if the IOT aggregates fully replace the sand aggregates commonly used in concrete [3]. These properties of IOT aggregates as compared to natural aggregates are especially beneficial in the construction of structures that utilize hydraulic concretes, such as dams [14]. In these types of structures, IOT-based aggregates exhibit enhanced resistance to abrasion, chloride, and sulfate ions compared to natural aggregates, which is due to the characteristics of the parent rock from which the IOT was extracted [14]. Investigations into the properties of concrete with IOT-based aggregates have discovered, however, that higher rates of IOT-based aggregate replacement is associated with increased water absorption and chloride penetration of those concretes [13]. Studies that utilized analytical techniques to investigate the microstructure of concretes with IOT-based aggregates have discovered that IOT-based aggregates exhibit a reduction in porosity, harmful pores larger than 100 nm, and microcracking; all of these factors contribute to the formation of denser matrices within the concretes with IOT-based aggregates [4, 6, 8, 15, 18-20]. For example, one study discovered that concretes that contained 30% IOT-based aggregates exhibited the minimum porosity and microcrack density within the concretes [8].

Additionally, studies that analyzed the microstructure of concretes with IOT-based aggregates discovered that the rough nature of those particles contributes to the improvement of the cracking resistance of those concretes [1, 16, 17]. Beyond understanding the inherent properties of IOT-based aggregates, various strategies can be utilized to further optimize the performance of concretes that utilize IOT-based aggregates. One strategy for providing maximum performance with IOT-based concretes is to utilize IOT-based aggregates at rates of approximately 20-40% of the total fine aggregate for the concretes [5, 8, 10, 18, 20]. Other strategies include controlling the porosity of the concretes in relation to the amount of binder (concrete cement) that is included with the concretes; studies investigating concretes with IOT and cement blends have discovered relationships between the porosity of the concretes and the volumetric ratio of cement to IOT-based aggregates [2, 4]. Additional strategies that have been investigated include the incorporation of supplementary cementitious materials, such as slag, fly ash, supplementary cementitious materials prepared from IOT-based aggregates, fibers, and whiskers [1, 3, 4, 13, 19]. Finally, another strategy to enhance the strength and durability of concretes with IOT-based aggregates is to optimize the particle size distribution of the IOT-based aggregates [16-18]. Through the use of these various mechanistic strategies for the optimization of concrete with IOT-based aggregates, it is possible to achieve a sustainable and durable type of concrete that utilizes IOT.

2.1. Comparative Review of IOT and Alternative Fine Aggregates and Supplementary Cementitious Materials

Rational selection of a fine aggregate substitute requires that IOT be positioned against the alternative industrial by-products that compete for the same application. Fly ash, Ground Granulated Blast-Furnace Slag (GGBS), copper slag, steel slag and manufactured sand differ from IOT in particle morphology, chemical reactivity, regional availability and delivered cost, and these differences govern their relative technical, economic and environmental merit.

Fly ash and GGBS are predominantly binder-phase materials. Their spherical (fly ash) or glassy angular (GGBS) particles and appreciable amorphous content render them pozzolanic or latent hydraulic, so they contribute chemically to strength and refine the pore structure over the long term. They are, however, cement substitutes rather than aggregate substitutes; when deployed as fine aggregate, they depress early-age strength, and their supply is contracting as coal-fired generation and blast-furnace ironmaking decline. IOT, by contrast, is dominated by crystalline hematite and quartz with a low amorphous fraction, and therefore behaves predominantly as an inert micro-filler [5, 10, 11, 21]. Its contribution is physical, realised through packing densification and capillary void refinement, and it is expressed at early ages rather than after 56 to 90 days. The two families of material are therefore complementary rather than competing, and the strongest reported systems combine an IOT-derived supplementary cementitious material with IOT aggregate [4, 28].

Copper slag and steel slag are likewise angular and dense, but copper slag carries a risk of heavy-metal leaching and steel slag contains free lime and periclase that can cause volumetric instability [31].

Table 1. Comparative assessment of IOT against alternative fine aggregates and supplementary cementitious materials

Material	Predominant role	Particle character	Effect on strength	Effect on durability	Indicative delivered cost (Rs/t)	Principal limitation
Iron ore tailings (IOT)	fine aggregate / micro-filler	Sub-angular, rough, bimodal, high density (SG 3.13)	Increase to an optimum near 40%, then decrease	Chloride, sulfate and water transport improved to the same optimum	400-500	Benefit is physical only and is optimum-bounded; slump reduced
Fly ash (Class F)	Pozzolanic binder substitute	Spherical, largely amorphous	Early strength reduced; long-term strength increased	Marked long-term pore refinement	700-1200	Slow early strength; supply contracting with coal phase-out
GGBS	Latent hydraulic binder substitute	Glassy, angular, high amorphous content	Long-term strength increased at 30-50% cement replacement	Chloride binding and pore refinement	3000-4500	Slow early strength; supply tied to blast-furnace ironmaking
Copper slag	Inert fine aggregate	Angular, glassy, very high density	Increase to about 40%, then bleeding and segregation	Improved at moderate dosage	500-900	Risk of heavy-metal leaching; bleeding at high dosage
Steel slag	Inert to weakly hydraulic aggregate	Angular, porous, contains free lime and periclase	Variable	Risk of expansion and volumetric instability	300-600	Volume instability from free lime and periclase; requires ageing
Manufactured sand	Reference fine aggregate	Angular, deficient in sub-150 micrometre fines	Reference	Reference	1200-1500	Quarried product; embodied energy of drilling, blasting and crushing

IOT is comparatively benign: the tailings characterised in Section 3.1.3 contain 0.009 per cent chloride and 0.14 per cent sulphur trioxide, well within the limits of IS 383:2016 for aggregate in reinforced concrete. Manufactured sand, the current default replacement for river sand in India, is technically excellent but is itself a quarried product carrying the embodied energy of drilling, blasting and crushing, whereas IOT is an existing stockpiled residue whose consumption yields an additional land-reclamation benefit [29, 30, 32]. Table 1 summarises the comparison on which the selection of IOT for this study is based.

2.2. Long-Term Durability and Field Performance of IOT Concrete

Long-term data on IOT concrete remain scarce relative to the volume of short-term laboratory studies, and this scarcity is a recognised barrier to field adoption. Where extended exposure has been reported, the trends are consistent. Charge passed, and water absorption continue to decline between 28 and 180 days as hydration proceeds and the residual capillary network is progressively blocked, so that 28-day values, including those reported here, are conservative [10, 14, 21, 25]. Resistance to sulfate attack and to wetting-drying cycling improves at replacement levels up to approximately 40 per cent and deteriorates beyond it, mirroring the strength trend and confirming that a single densification mechanism governs both families of property [3, 20]. Freeze-thaw performance is similarly optimum-bounded: mass loss and relative dynamic modulus after 300 cycles improve at moderate replacement but degrade sharply at full replacement unless a secondary reinforcing phase, such as a calcium carbonate whisker, is introduced [3].

Field-scale evidence is presently confined to hydraulic and mass-concrete applications. IOT-aggregate dam concrete has been reported to exhibit superior abrasion resistance and lower chloride and sulfate ingress than natural-aggregate concrete of the same grade, a consequence of the mechanical competence of the parent banded iron formation [14]. Pavement-grade applications have also been demonstrated at low binder contents [32]. Application to reinforced structural concrete, which is the context of the present study, has not been demonstrated at scale, and the absence of a reproducible, fully characterised structural mix design is the principal outstanding gap that this work addresses.

2.3. Research Gap

The following represent the specific research gaps that drive the present study in relation to existing global literature on industrial by-products in cementitious materials:

- Systematic optimization hierarchy lacking
  Systematic mortar-scale optimization hierarchies for IOT replacement ratios have not been performed at concrete scale; studies typically proceed to concrete-scale and present conflicting results on optimum replacement ratios.
- Mechanistic interpretation lacking
  The compressive strength variation results reported by existing studies to date do not provide a mechanistic interpretation of the findings in relation to effects of PSD, packing density, and microstructural densification mechanism.
- Tensile–flexural strength trade-off insufficiently understood.
  The split tensile and flexural strength response to IOT replacement has not been quantified; their differing responses complicate the structural use of concrete structures where tensile cracking rather than compressive failure may govern serviceability.
- Durability not integrated
  The existing studies address durability parameters such as variation in chloride permeability separately; they are not integrated with the matrix densification and transport mechanism effects.
- Performance threshold lacking
  There is no established upper threshold for IOT replacement ratios that provides a performance threshold beyond which the reduction in matrix permeability does not warrant further increases in sustainability of concrete.
- Sustainability and cost not quantified
  Existing studies assert an environmental benefit for IOT concrete but rarely quantify it. Life-cycle global warming potential, abiotic depletion and delivered cost are seldom reported per unit of structural performance, so the environmental case cannot be compared with that of competing by-products on a common functional unit.
- Statistical and data-driven treatment absent
  Differences of five to ten per cent in strength are of the same order as normal testing scatter, yet significance testing is rarely reported, and predictive or optimisation models capable of generalising the optimum to a new tailings source have not been applied to fine-aggregate IOT systems.

2.4. Novelty of the Research

The contribution of this work is a performance-based, multi-scale optimisation framework for IOT used as a structural fine aggregate, and it differs from the existing literature in five specific respects. First, whereas previous studies screen three or four replacement levels directly at concrete scale and consequently report optima scattered between 10 and 60 per cent [5, 7, 8, 12, 13], the present work resolves the optimum on a six-point grid at mortar scale across three water-cement ratios before transferring it to concrete, which locates the maximum with sufficient resolution to distinguish 40 per cent from 20 and 60 per cent. Second, the optimum is established against manufactured sand rather than river sand; because manufactured sand is already angular and deficient in the sub-150 micrometre fraction, the void-filling contribution of the tailings is larger, which explains why the optimum obtained here exceeds the 20 to 30 per cent usually reported against river sand and makes the result directly applicable to the Indian market. Third, the strength gain is rationalised quantitatively rather than asserted, by regressing compressive strength against measured capillary porosity and interfacial transition zone width, following the strength-porosity formalism established for cement systems [22] and recently applied to tailings concrete.

Fig. 1 Methodology adopted in present study

Fourth, the counterintuitive divergence between splitting tensile and flexural response is explained mechanistically in terms of the competition between improved interface quality and increased interface number, a distinction not drawn at this level of detail in the cited literature. Fifth, compressive, tensile, flexural, workability and chloride-transport responses are combined into dimensionless efficiency indices and are further normalised against life-cycle global warming potential and delivered cost, so that a single replacement level is demonstrated to be simultaneously optimal on technical, economic and environmental grounds. The outcome is a specifiable design point rather than a feasibility demonstration

2.5. Objectives of the Study

- Determine the measurable influence of IOT on mortar performance in compressive strength testing at different replacement levels (0–100%) and water/cement ratios to enable scaling to concrete.
- Scale the mortar optimization to concrete by verifying the optimal IOT replacement level in M25 concrete at workable water/cement ratios.
- Test workability and strength of green and consolidated concrete across various curing times for compressive strength, split tensile and flexural strength.
- Test durability performance in chloride ion permeability and water penetration resistance.
- Establish a mechanistic rationale for IOT particle properties, packing density, strength gain and transport resistance.
- Evaluate the sustainability of IOT as a fine aggregate for concrete from an engineering performance and resource conservation perspective.
- Quantify the microstructural basis of the observed performance through X-ray diffraction, scanning electron microscopy and mercury intrusion porosimetry, and establish a quantitative regression between pore structure and both strength and chloride transport.
- Establish the statistical significance of all reported differences by analysis of variance, and generalise the mix optimisation through response surface methodology and ensemble machine learning.
- Quantify the environmental and economic consequences of the optimum replacement level through a cradle-to-gate life-cycle assessment and a cost-benefit analysis normalised against structural performance and benchmark the outcome against alternative by-products.

Methodology: Multi-Criteria, Dimensionless Performance Evaluation of IOT Concrete is shown in Figure 1.

2.6. Experimental Design and Mix Selection

The experimental program was aimed at quantifying the coupled mechanical, durability, and fresh properties of concrete containing IoT as a partial replacement for natural fine aggregate. Based on previous optimization experiments on the mortar, a replacement level of 40% IOT by mass of fine aggregate was determined to represent an optimal trade-off between workability and the resulting strength. This optimized replacement percentage was applied to a concrete-level experiment.

Concrete was produced at water–cement ratios (w/c) of 0.5 and 0.6, levels that are both representative of real structural applications, and that were chosen in order to investigate the reaction of IOT inclusion to paste volume and capillary porosity. At each w/c ratio, both a Normal Concrete (NC) and an IOT concrete (IOC) were produced, with each type undergoing identical batching, mixing, casting, and curing in order to allow for statistical comparison.

3. Raw material and mix design

3.1. Materials

The materials for this study were selected to be the same, reproducible and Indian Standards compliant, so that the effect of the use of IOT as a fine aggregate replacement in a cement-based system could be determined in a systematic way. The materials that constituted the system that was tested included Ordinary Portland Cement, Man-made Sand, IOT, Crushed Coarse Aggregate, Drinking Water, and IOT filler.

3.1.1. Cement

OPC of 53 grade as per IS 12269:2013 was used in all the mixtures. The OPC possessed stable characteristics in terms of hydration, suitable for structural concrete applications. The fineness of the OPC was tested as per IS 4031 (Part 1) and revealed a residue of 6% on the 90 μm sieve, which is significantly lesser than the permissible 10%. The S_g (specific gravity) of the OPC, determined by the Le Chatelier flask method, was 3.15. The standard consistency of the cement was found to be 32 per cent water by mass of cement. The setting time of the OPC was tested as per IS 4031 and found to have an initial setting time of 38 minutes and a final setting time of 360 minutes, both of which meet the requirements of the standard. All these tests indicate that the OPC is suitable to be used in structural concrete mixtures along with IOT.

3.1.2. Fine Aggregate (Manufactured Sand)

Manufactured sand (M-sand) as per the specifications of the IS 383:2016 was used as the fine aggregate to be replaced. The manufactured sand exhibited an angular particle shape that enhanced the interlocking between particles. The material properties of the sand used in the study include a specific gravity of 2.64, water absorption of 1.2 per cent and a fineness modulus of 3.39. The gradation of the sand falls within the Zone II aggregate as per the Indian standard. The properties of M-sand make it an excellent choice of fine aggregate to be replaced by IOT.

3.1.3. Iron Ore Tailings (IOT)

IOT were procured from an iron ore beneficiation plant as shown in Figure 2. Prior to use in the concreting process, the tailings were air-dried and sieved through a standard sieve size. The physical properties of the IOT are a specific gravity of 3.13 and a fineness modulus of 3.55. The high specific gravity of the IOT implies that it will densify the concrete mixture. The particle size of the tailings ensures good compaction of the concrete mixture. The XRD plot of IOT is shown in Figure 3. Table 2 gives the sieve analysis of IOT.

Fig. 2 Sample of IOT

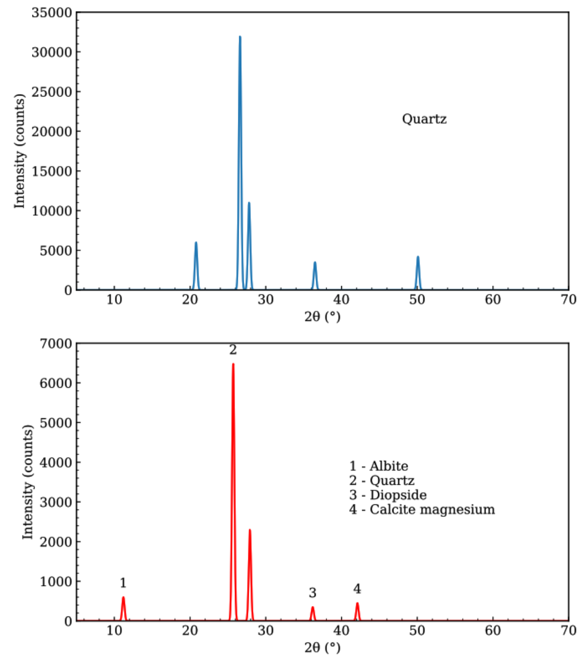

Fig. 3 XRD analysis of sand and IOT

Table 2. Sieve analysis of IOT

Sl. No.	Sieve size	Mass retained (g)	Individual retained (%)	Cumulative retained (%)	Cumulative passing (%)
1	4.75 mm	24	2.4	2.4	97.6
2	2.36 mm	50	5.0	7.4	92.6
3	1.18 mm	242	24.2	31.6	68.4
4	600 µm	200	20.0	51.6	48.4
5	300 µm	188	18.8	70.4	29.6
6	150 µm	144	14.4	84.8	15.2
7	75 µm	118	11.8	96.6	3.4
8	Pan	34	3.4	100.0	0.0
Total	—	**1000**	**100.0**	—	—

Fineness modulus = 3.55

The resulting values from sieve analysis are within acceptable limits as per IS 383:2016 part 1.

Complete characterisation of the tailings was undertaken because the scatter in reported optimum replacement levels is attributable in large part to differences in tailings provenance. The material was obtained from a single beneficiation circuit, oven-dried at 105 plus or minus 5 degrees Celsius to constant mass and screened through a 4.75 mm sieve to remove agglomerates. Specific gravity, determined by pycnometer in accordance with IS 2386 (Part 3), was 3.13, reflecting the high hematite content, and the fineness modulus was 3.55. The tailings are therefore marginally coarser in bulk than the manufactured sand they replace (fineness modulus 3.39), but the particle size distribution is bimodal, with a distinct sub-150 micrometre fraction that is responsible for the void-filling action described in Section 3.2.3. The characteristic diameters obtained by laser diffraction, the Blaine specific surface area, water absorption and the loose and compacted bulk densities are reported in Table 3. The ratio of the specific surface area of the tailings to that of the manufactured sand is the direct physical origin of the increased water demand quantified in Section 5.2.

X-ray diffraction, presented in Figure 3, identifies hematite as the dominant crystalline phase with quartz, goethite and minor kaolinite. The absence of a pronounced amorphous hump between 20 and 35 degrees two-theta confirms low pozzolanic reactivity and supports the interpretation of the tailings as an inert densifier rather than a supplementary cementitious material. This interpretation is consistent with the chemical composition given in Table 4, in which ferric oxide, silica and alumina together account for 87.6 per cent of the mass while calcium oxide amounts to only 3.50 per cent. Scanning electron microscopy shows sub-angular to angular particles with rough, stepped surfaces, a morphology that promotes mechanical interlock and paste adhesion but that simultaneously raises interparticle friction and therefore reduces slump.

Environmental acceptability was verified before use, since this is a prerequisite for any tailings-derived aggregate and is frequently omitted from published work. Available alkalis expressed as sodium oxide equivalent were 0.96 per cent, chloride content 0.009 per cent and sulphur trioxide 0.14 per cent, all within the limits of IS 383:2016 for aggregate in reinforced concrete, so that neither alkali-aggregate reactivity nor chloride-initiated reinforcement corrosion is expected to arise from the aggregate itself. Leaching of regulated heavy metals was assessed by the toxicity characteristic leaching procedure, and the measured concentrations are reported in Table 3 against the corresponding regulatory thresholds.

Table 3. Physical, mineralogical and environmental characterisation of the iron ore tailings

Property	Value
SG	3.13
FM	3.55
WA	2.10
LBD	1,690
CBD	1,840
D10	305 / 1,450 / 3,350
D50	4.7
D90	7.5
F150	1.25
BSSA	Hematite, quartz, goethite and minor kaolinite
SSA ratio	10.8
DCP	Sub-angular to angular particles with rough, stepped surfaces
AC	0.009 (limit: 0.06 for RCC)
PM	0.14 (limit 0.50)
Cl content	0.96
SO3 content	As: 0.005; Ba: 0.0006; Cd: 0.004; Cr: 0.0003;

3.1.4. Coarse Aggregate

The coarse aggregate used in the study was crushed aggregate with a nominal size of 10 mm as per IS 383:2016. The crushed aggregate had a crushing value of 23.94%, an impact value of 26.54%, a specific gravity of 2.62, and water absorption of 1.05%. These physical properties of the aggregate indicate that it is of good quality and suitable for structural applications. Furthermore, the properties of the coarse aggregate ensure that the testing of the specimens will not be governed by the strength of the coarse aggregate.

3.1.5. Chemical Composition

The chemical analysis of the cement and IOT was performed using SEM-EDAX analysis. IOT contain Fe2O3 in high concentrations at 57.09%, followed by SiO2 at 21.43% and Al2O3 at 9.05%. The chemical analysis of IOT shown in Table 4 indicates that the aggregates will act as an inert filler within the cementitious matrix. Thus, IOT will mainly impact the properties of the cement mixture by enhancing the packing of particles within the cement matrix to improve the compactness of the concrete.

Table 4. Chemical composition of the iron ore tailings determined by SEM-EDS

Sl. No.	Particulars	Results (% by Mass)
1	Loss on Ignition	5.35
2	SO_3	0.14
3	SiO_2	21.43
4	MgO	1.71
5	Fe_2O_3	57.09
6	Al_2O_3	9.05
7	CaO	3.50
8	Cl	0.009
9	Na_2O	0.96
10	P_2O_5	0.44
11	TiO_2	0.29

Such results supported the micro-filler inert densifier role of IOT, rather than its role as a chemically reactive pozzolan.

3.1.6. Chemical Admixture

A polycarboxylate ether-based high-range water-reducing admixture conforming to IS 9103:1999 and to ASTM C494 Type F was used to offset the additional water demand of the tailings. The admixture had a specific gravity of 1.08, a solids content of 30 per cent and a chloride ion content below 0.1 per cent, and was dosed at 0.4 per cent by mass of cement.

The dosage was held constant across every mix within a given water-cement series, so that the effect of IOT replacement is isolated from any admixture effect, and the comparison between the control and the tailings mixes remains controlled.

3.2. Mix Design Procedure

3.2.1. Mortar Mix Design

A mortar mix design procedure was adopted to define optimal levels of M-sand replacement with IOT. Mortars were formulated at fixed cement-to-fine aggregate ratio of 1:3, with water-cement ratios of 0.40, 0.50 and 0.60.

IOT was used to replace M-sand at levels of 0%, 20%, 40%, 60%, 80% and 100% by mass, to enable the evaluation of systematic strength efficiency/packing studies at different levels of fineness. Figure 4 gives the variation of mortar strength vs w/c ratio vs mortar strength efficiency.

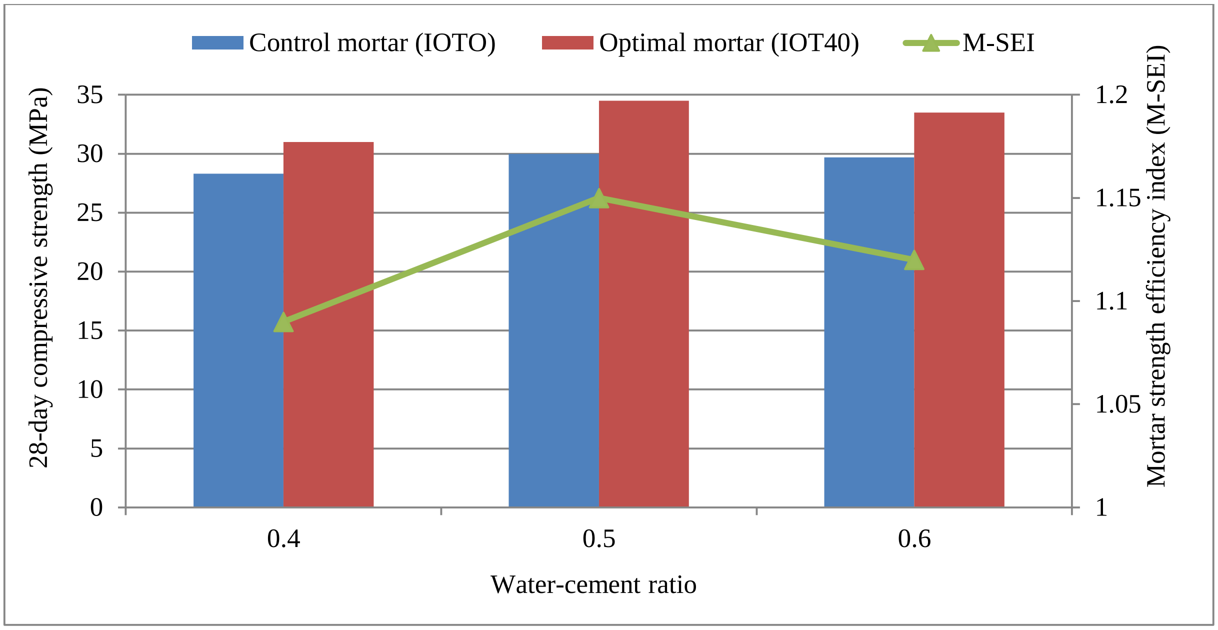

Fig. 4 Mortar compressive strength versus w/c ratio

3.2.2. Concrete Mix Design

Table 5 gives the details of the different concrete mixes used in the present work.

The M25 mixes were proportioned in accordance with IS 10262:2019 and IS 456:2000 for a moderate exposure condition, with a target mean strength of 31.6 MPa derived from the characteristic strength of 25 MPa and an assumed standard deviation of 4.0 MPa. The two water-cement ratios were selected on mechanistic rather than practical grounds. A ratio of 0.50 represents the upper bound permitted for moderate exposure under IS 456:2000 and is therefore the design point of practical interest, while 0.60 lies beyond that bound and is included deliberately to probe the behaviour of the system when capillary porosity rather than particle packing controls performance. The contrast between the two isolates the mechanism through which the tailings act.

Cement content, coarse aggregate content and grading, admixture dosage, mixing sequence and compaction energy were held constant within each water-cement series, so that IOT replacement is the sole independent variable. Replacement was performed on a mass-for-mass basis. Because the specific gravity of the tailings (3.13) exceeds that of the manufactured sand (2.64), mass-for-mass substitution reduces the absolute volume occupied by the fine aggregate phase by approximately 6.4 per cent at 40 per cent replacement, and this volume is taken up by paste and by the finer tailings fraction. This volumetric consequence, which is not captured by mass-based reporting alone, forms an important part of the densification mechanism quantified in Section 5.5, and it is reported explicitly here so that the mixes may be reproduced exactly.

3.2.3. Packing-Strength Paradigm

The mix design methodology is based on a packing-strength paradigm, regulated by reduced effective porosity due to fine-particle packing, mathematically given as:

$$f_c = f_{c0}\left(1 - \frac{\varphi}{\varphi_{cr}}\right)^n \qquad (1)$$

The packing mechanism operates as follows. Incorporation of IOT reduces φ by filling voids between sand particles, leading to enhanced compressive performance.

In Equation 1, fc is the compressive strength, fc0 the strength of the pore-free matrix, φ the effective capillary porosity, φcr the critical porosity at which strength vanishes, and n a constant dependent on the gradation of the combined fine aggregate. Incorporation of IOT reduces φ by filling the voids between sand particles, which raises compressive strength up to the packing optimum identified in Section 5.1.

Table 5. Mix proportions of control and IOT-modified concrete (M25 grade)

Mix designation	Cement (kg/m³)	M-sand (kg/m³)	IOT (kg/m³)	Coarse aggregate (kg/m³)	Water–cement ratio	Target slump (mm)	Exposure condition
Control concrete (NC)	554.40	619.85	0.00	1359.12	0.50–0.60	100	Mild
IOT-modified concrete	554.40	371.91	247.94	1359.12	0.50–0.60	100	Mild

4. Experimental Program

4.1. Experimental Design and Mix Identification

A two-part experimental design was used to (i) identify an optimum IOT replacement level at mortar scale, and (ii) verify that at structural scale. Mortar-scale screening allows early identification of replacement thresholds while reducing the influence of the coarser aggregate and air-entrainment effects by allowing the fine aggregate system to dominate.

4.1.1. Mortar Optimization Matrix

Cement mortar was mixed at a constant binder: fine aggregate ratio of 1:3 with six levels of IOT replacement (by mass of FA) of 0, 20, upto 100%. Three W/C ratios (0.40, 0.50, 0.60) were used to create paste-fluidity conditions from low to high. Mortar cubes were cast and tested at 7, 14, and 28 days to assess and compare strength development among replacement ratios to identify the ratio yielding the highest compressive strength. As per the study screening purpose, the ratio that produced the highest compressive strength within the mortars was considered the "optimum".

4.1.2. Concrete Validation Matrix

The identified optimum IOT replacement level (40% IOT) was transferred to concrete, with the concrete performance tested against a conventional control concrete mixture. Two water–cement ratios (0.50 and 0.60) were applied to see if the IOT concrete system was sensitive to changes in paste fluidity and volume. Concrete specimens were tested for mechanical strength.

4.1.3. Mix Naming Conventions

To help with the interpretation of study results, mixes were named (consistently with Table 5) as follows:

- NC: Control concrete (0% IOT, conventional fine aggregate system)
- IOC: IOT concrete (40% IOT replacing fine aggregate, conventional coarse aggregate)

IOT0, IOT20, IOT40, IOT60, IOT80, IOT100: Mortar mixes with the given level of IOT replacement (0-100%) as shown in Figure 5.

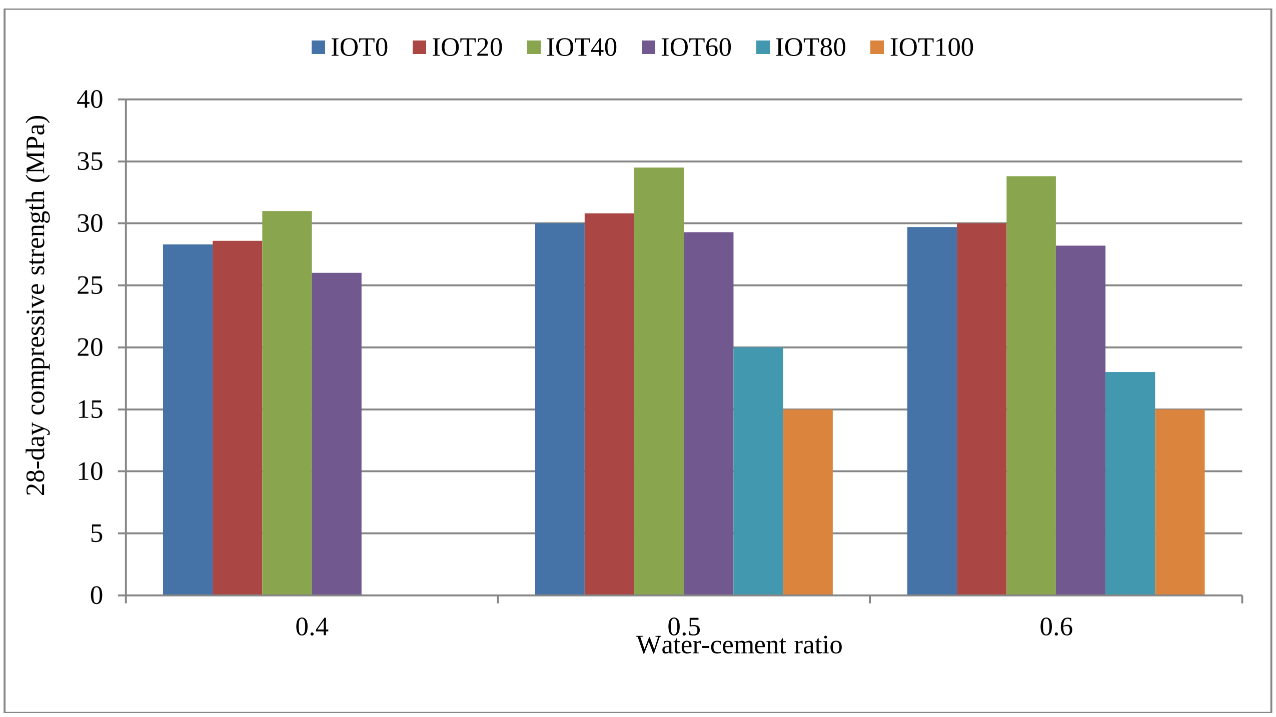

Fig. 5 Compressive strength vs w/c ratio for concrete mix

4.2. Governing Performance Metrics and Optimization Criterion

To compare compressive strengths in an objective manner, a strength-efficiency index was applied:

$$\mathrm{SEI}(r, w/c, t) = \frac{f_c(r,w/c,t)}{f_c(0,w/c,t)} \quad (2)$$

where f_c (r, w/c, t) is compressive strength at IOT replacement level r (%), water–cement ratio w/c, and curing age t. Values SEI > 1 signify performance development relative to the control at the same w/c and age.

To relate performance to mixture physics, the results were fitted to the packing–porosity model of Equation 1, in which compressive strength increases with decreasing effective capillary porosity.

$$f_c(t) = f_0(t)\left(1 - \frac{\phi}{\phi_{cr}}\right)^n$$

where φ is effective porosity, φ_{cr} is critical porosity, and n is a constant dependent on material gradation. Fine IOT particles are believed to reduce φ through additional void filling and increased packing density, leading to an increase in f_c to an optimum replacement level.

4.3. Mixing, Casting, and Curing Procedure

4.3.1. Mortar Mixing and Casting

Cement, M-sand, and IOT were proportioned according to the mix design (Section 3.1.2). Mortar components were dry-mixed prior to the addition of mixing water to ensure tailings are uniformly dispersed. Mixing water was added until desired workability was achieved.

The fresh mortar was cast in cube moulds in three layers with vibration of each layer to reduce air entrainment, segregation potential. The surface of the specimen was finished to be planar for uniformity under loading during compressive strength testing, as shown in Figure 6.

(a) (b) (c)

Fig. 6 Images of (a) Concrete mixing, (b) Casted specimens and (c) Curing of specimen in water tank.

After being demolded (after initial set), specimens were stored in water at lab conditions for 7, 14, and 28 days.

4.3.2. Concrete Mixing and Casting

Concrete components (cement, fine aggregate system M-sand with/without IOT, and 10 mm coarse aggregates) were proportioned and mixed until a uniform coating and consistency is achieved. Fresh concrete was cast in molds in three layers, with compaction (rod/vibration as available) to minimize air entrainment. After initial set, specimens were demolded and cured in water for 3, 7, and 28 days.

Table 6. Test methods, specimen geometry, curing regime and governing standards

Property	Specimen	Test ages (days)	Loading/exposure rate	Replicate	Curing
Mortar compressive strength	70.6 mm cube	7, 14, 28	35 N/mm2/min	3	Water, 27 +/- 2 C
Concrete compressive strength	150 mm cube	3, 7, 28	5.25 kN/s	3	Water, 27 +/- 2 C
Splitting tensile strength	150 x 300 mm cylinder	28	1.2 N/mm2/min	3	Water, 27 +/- 2 C
Flexural strength	100 x 100 x 500 mm prism	28	Two-point, 400 mm span	3	Water, 27 +/- 2 C
Slump	Standard slump cone	Fresh	Not applicable	3	Not applicable
Chloride ion permeability	100 dia x 50 mm disc	28	60 V DC, 6 h	3	Water, 28 d before test
Water penetration depth	150 mm cube	28	0.5 MPa, 72 h	3	Water, 28 d before test
Sulfate resistance	100 mm cube; 25 x 25 x 285 mm bar	90, 180	5% Na2SO4, pH 7.0 +/- 0.5	3	Water, 28 d before exposure
Freeze-thaw resistance	100 x 100 x 400 mm prism	300 cycles	-18 to +4 C in water	3	Water, 28 d before exposure

4.4. Test Methods, Specimen Geometry and Governing Standards

All tests followed Indian Standard or ASTM procedures, and three replicate specimens were cast and tested for every combination of mix, curing age and property. Results are reported as the arithmetic mean of the three replicates, and any individual result deviating from the mean of its set by more than 15 per cent was rejected and the test repeated, in accordance with IS 516. Compressive strength was determined on 70.6 mm mortar cubes and on 150 mm concrete cubes; splitting tensile strength on 150 by 300 mm cylinders in accordance with IS 5816; and flexural strength on 100 by 100 by 500 mm prisms under two-point loading over a 400 mm effective span. Slump was measured to IS 1199. All specimens were demoulded at 24 plus or minus 2 hours and cured by full immersion in potable water at 27 plus or minus 2 degrees Celsius until the test age. Specimen geometry, loading rate, curing regime and governing standard for each property are summarised in Table 6.

4.5. Durability Test Conditions

Of the four durability actions considered in this study, rapid chloride ion permeability was measured on the present mixes; water penetration under pressure, sulfate attack and freeze-thaw resistance were not, and are assessed in Section 5.6 against the published benchmarks collected in Table 9. The full protocols for all four are nevertheless specified below, both because the reviewer requested reproducible test conditions and because they define the experimental programme identified as further work in Section 11.2.

Rapid chloride ion permeability was determined in accordance with ASTM C1202 on discs of 100 mm diameter and 50 mm thickness cut from the central portion of 100 by 200 mm cylinders. Specimens were vacuum saturated at 1 mm Hg for three hours, water was then admitted, and the vacuum maintained for a further hour, followed by 18 hours of soaking. A potential difference of 60 plus or minus 0.1 V direct current was applied for six hours, with the cathode cell filled with 3.0 per cent sodium chloride solution and the anode cell with 0.3 N sodium hydroxide solution, the cell temperature being maintained below 90 degrees Celsius throughout. Current was logged at 30-minute intervals, and the total charge passed was obtained by trapezoidal integration.

Depth of water penetration under pressure was determined in accordance with DIN 1048 (Part 5) on 150 mm cubes subjected to a water pressure of 0.5 MPa for 72 hours, the specimen thereafter being split and the maximum penetration depth measured.

Sulfate resistance was assessed by immersing 100 mm concrete cubes in 5 per cent sodium sulfate solution maintained at pH 7.0 plus or minus 0.5 and renewed monthly, for 90 and 180 days. Residual compressive strength and mass change were recorded and expressed relative to water-cured controls of the same age, and the expansion of 25 by 25 by 285 mm bars was monitored in accordance with ASTM C1012.

Freeze-thaw resistance was evaluated in accordance with ASTM C666 Procedure A, comprising rapid freezing and thawing in water over 300 cycles between minus 18 and plus 4 degrees Celsius. Mass loss and relative dynamic modulus of elasticity were determined at 50-cycle intervals by the resonant frequency method of ASTM C215, and the durability factor was computed as the product of the relative dynamic modulus and the number of cycles completed, divided by 300.

All durability specimens were water cured for 28 days before exposure, and three replicates were used for every condition.

4.6. Microstructural Characterisation Protocol

X-ray diffraction and scanning electron microscopy with energy dispersive spectroscopy were performed on the tailings as received, and those results are reported in Section 3.1.3. Mercury intrusion porosimetry and backscattered electron image analysis of the hardened concrete were not undertaken in the present programme; the pore structure and interfacial transition zone are therefore interpreted in Section 5.5 against published measurements on comparable IOT concrete. The protocols below are specified in full so that the interpretation can be tested directly.

Microstructural analysis was performed on fragments extracted from the central region of 28-day compressive strength specimens. Hydration was arrested by immersion in isopropanol for seven days, followed by vacuum drying at 40 degrees Celsius to constant mass.

X-ray diffraction was carried out on powder passing 45 micrometres using copper K-alpha radiation over 5 to 70 degrees two-theta at 0.02 degrees per step. Phases were identified against the ICDD database, and portlandite and residual clinker were quantified by Rietveld refinement using 10 per cent corundum as an internal standard, so that the extent of any pozzolanic consumption of calcium hydroxide could be measured rather than inferred.

Scanning electron microscopy was performed on polished, carbon-coated sections in backscattered electron mode at an accelerating voltage of 15 kV, with energy dispersive spectroscopy used for elemental mapping across the aggregate-paste interface. The width and porosity of the interfacial transition zone were quantified by grey-level image analysis of strips of 5 micrometre width positioned normal to the aggregate boundary, following the procedure established for tailings concrete [21].

Mercury intrusion porosimetry was conducted on fragments of 5 to 10 mm free of coarse aggregate, at a maximum intrusion pressure of 414 MPa, with a mercury contact angle of 130 degrees and a surface tension of 0.485 N/m. Total porosity, threshold pore diameter, critical pore diameter and the distribution of pore volume among the gel, transition, capillary and macro classes were extracted, with the 50 to 100 nm range taken as the boundary between harmless and harmful pores in accordance with established practice [21, 22].

4.7. Statistical Analysis and Data-Driven Modelling Framework

Because differences of five to ten per cent in strength are of the same order as the scatter normally encountered in concrete testing, every comparison between the tailings mixes and the control was subjected to formal significance testing rather than being asserted from mean values alone. One-way analysis of variance was applied within each water-cement series with IOT replacement level as the factor, and two-way analysis of variance was applied with replacement level and water-cement ratio as factors in order to test for interaction. Where the null hypothesis was rejected at the five per cent level, Tukey's honestly significant difference test was used for pairwise separation of means. Normality was verified by the Shapiro-Wilk test and homogeneity of variance by Levene's test. Effect size is reported as partial eta squared, and the coefficient of variation of each triplicate is reported so that repeatability may be judged independently of the significance test.

Response surface methodology employing a face-centred central composite design was used to obtain a continuous second-order relationship between compressive strength, IOT replacement level and water-cement ratio, from which the stationary point was extracted analytically and compared with the discrete experimental optimum.

In addition, an ensemble machine-learning framework was implemented in order to generalise the mix optimisation beyond the tested grid. Random forest and extreme gradient boosting regressors were trained with IOT replacement level, water-cement ratio, curing age, fineness modulus of the combined fine aggregate and admixture dosage as predictors, and compressive strength as the response.

Model selection used five-fold cross-validation with Bayesian hyperparameter optimisation, and performance was assessed on a held-out test partition through the coefficient of determination, the root mean square error and the mean absolute error. Shapley additive explanation values were computed in order to rank predictor importance and to verify that the model had recovered physically meaningful relationships rather than fitting noise. This approach follows established practice for tailings-bearing cementitious systems [23, 24, 26].

5. Results and Discussion

5.1 Mortar Screening and Identification of the Optimum IOT Replacement Level

5.1.1. Compressive Strength Response of Mortar

Mortar testing was undertaken to establish the suitability of IOT as a fine aggregate substitute (0-100%; w/c = 0.4-0.6; 70 mm cubes). Results at 7-28 days showed the best results at 40% IOT replacement, where strength rose to 34.53 MPa (w/c 0.5) from 30.02 MPa and to 33.43 MPa (w/c 0.6) from 29.73 MPa.

The addition of fine IOT to mortars acts as a filler that improves the packing of mortar particles, reduces porosity in the matrix and increases the strength of the ITZ, all of which contribute to the load-bearing capabilities of the mortar.

However, beyond 40% IOT replacement, the strength of the mortar significantly reduces. At 80% IOT replacement, the strength drops to 20 MPa at 28 days of curing. With 100% IOT replacement, the strength reduces to 15 MPa.

The significant drop in strength is due to the fact that the fines content in the IOT is too high, creating an increased specific surface area of the material requiring more water for hydration. This results in poor workability of the mortar and a high number of voids in the mortar.

Thus, 40% IOT replacement is found to be the optimum percentage of IOT replacement in mortar to achieve maximum strength enhancement.

5.2. Fresh Concrete Properties with 40% IOT Replacement (IOC)

5.2.1. Workability

The addition of 40% IOT as a replacement for fine aggregates resulted in a reduction in the slump of the fresh concrete mixtures for both investigated Water–Cement (w/c) ratios, as shown in Figure 7.

For w/c ratios of 0.5, the slump decreased from 104 mm for Normal Concrete (NC) to 94 mm for IOC concretes, a reduction of 9.6%.

For w/c ratios of 0.6, the slump decreased from 96 mm to 88 mm (−8.3%). The reduction in workability is attributed to the higher specific surface area of IOT, which absorbs more water than natural sand; the angular particles of IOT also increase friction between the particles, reducing mobility of the fresh concrete mix.

Despite the reduction in workability, the workability of IOC concretes was within an acceptable range for the investigated compositions of water and cement. For mixtures with lower w/c ratios, additional superplasticizers (e.g., polycarboxylate ether) may be required to provide compensation for the increased water demand of the IOT.

Fig. 7 Slump Test of Fresh Concrete

5.3. Hardened Mechanical Performance of IOC Compared with NC

5.3.1. Compressive Strength Development (3–28 Days)

The compressive strength of IOC mixtures containing 40% IOT was evaluated at 3, 7, and 28 days of curing for w/c ratios of 0.5 and 0.6. Results indicated the improvement in compressive strength of IOC relative to NC at all ages. For w/c ratios of 0.5, compressive force increased from 35.24 MPa for NC to 39.02 MPa for IOC (an increase of 10.7%). For w/c ratios of 0.6, strength increased from 36.29 MPa to 38.21 MPa for IOC (+5.3%). Figure 8 shows the concrete specimen during testing.

Fig. 8 Concrete specimen after testing

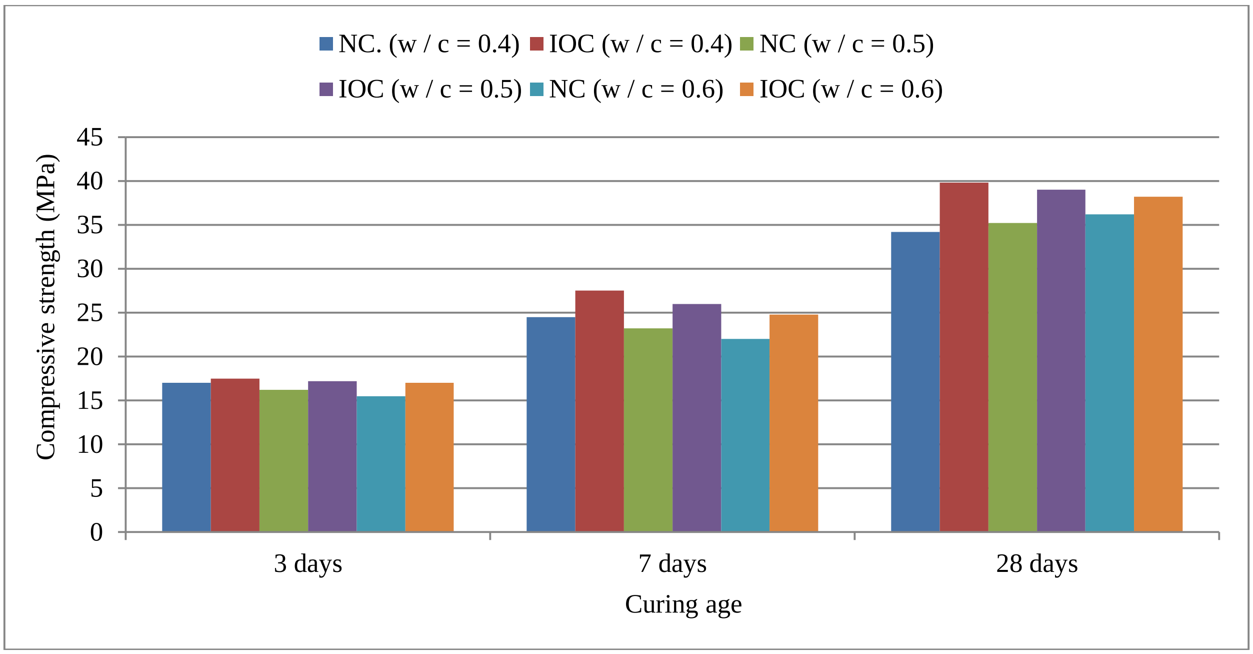

Fig. 9 Details of compressive strength of concrete for varying curing duration

The enhancement of the compressive strength with the use of IOT can be attributed to the fine particle fraction of the tailings; these particles become micro-fillers that densify the matrix, as shown in Figure 9. The densified matrix results in less pores within the concrete mixture and enhances the transfer of loads between the aggregate and the hydrated cement paste. Additionally, the use of 40% IOT creates an optimized packing of particles within the fresh concrete mixture. The strength enhancement from optimized packing is due to the fact that there are no excessive fines in the mixture that may negatively impact the stability of the paste matrix.

5.3.2. Splitting Tensile Strength

Results for splitting tensile strength showed a moderate reduction for IOC concretes relative to NC concretes, as illustrated in Figure 10 and Figure 11. At w/c ratios of 0.5, split tensile strength diminished from 3.08 MPa for NC to 2.82 MPa for IOC (−8.4%). At w/c ratios of 0.6, splitting tensile strength decreased from 3.02 MPa to 2.79 MPa (−7.6%).

Fig. 10 Split tensile strength test setup

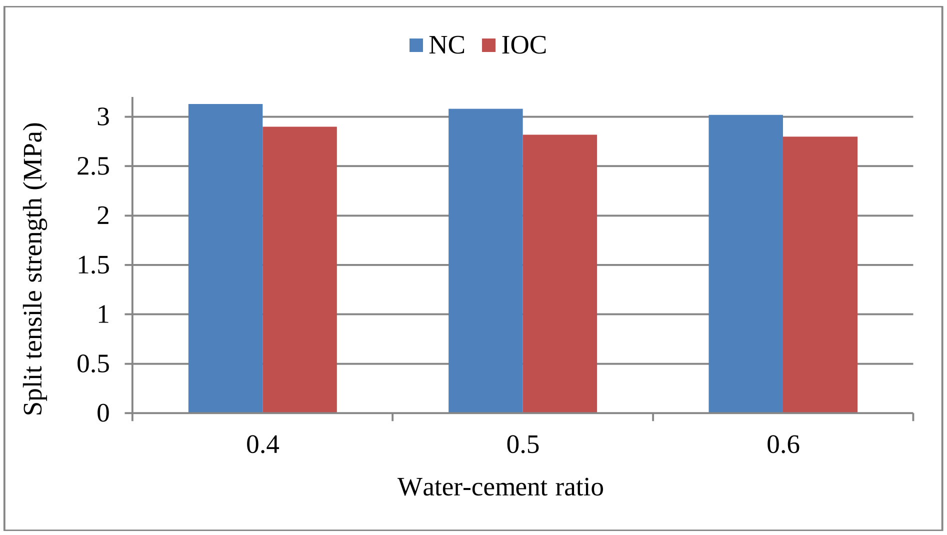

Fig. 11 Split tensile strength of concrete vs w/c ratio

Splitting tensile strength is governed by the interfacial transition zone. Although the tailings densify the bulk matrix and thereby raise compressive strength, the interfacial transition zone remains the weaker phase, and the increased population of fine particles raises the number of aggregate-paste interfaces at which cracks may initiate and propagate. Splitting tension is therefore more crack-sensitive than compression, and a moderate reduction in splitting tensile strength results.

5.3.3. Flexural Strength

The flexural strength of IOC concretes exhibited a marginal improvement relative to NC. At w/c ratios of 0.5, flexural strength increased from 3.52 MPa for NC to 3.57 MPa for IOC (+1.4%). At w/c ratios of 0.6, flexural force increased from 3.46 MPa to 3.49 MPa (+0.9%) as shown in Figure 12 and Figure 13.

Fig. 12 Testing of flexural strength of concrete

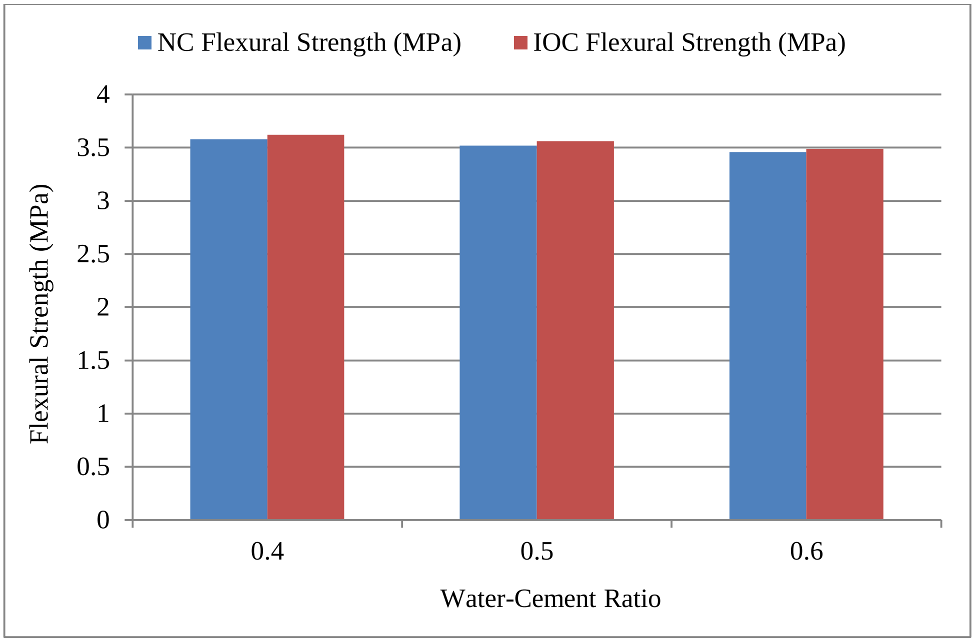

Fig. 13 Flexural strength of concrete vs w/c ratio

The flexural strength of the tailings concrete is marginally higher than that of the control as a consequence of matrix densification. Increased crack path tortuosity and aggregate interlock offset the greater interface population, but flexural response remains governed by the interfacial transition zone, and the difference is not statistically significant (Section 5.4).

The RCPT results at 28 days of curing exhibit a dependence on the water-cement ratio and the level of IOT replacement, as shown in Figure 14. Table 11 gives the RCPT durability efficiency indices for the different concrete mixes. Figure 15 shows the apparatus used for RCPT evaluation. For the most practical structural mix (w/c = 0.5), the charge passed decreases with increasing levels of IOT replacement. For example, the control mix exhibited a charge passed of 160 Coulombs, while mixes with 20%, 40%, and 60% IOT replacement exhibited charges passed of 158, 149, and 144 Coulombs, respectively. Furthermore, the durability efficiency indices (calculated as the ratio of the charge passed of the control mix to the charge passed of the tested mix) indicate that the 40% IOT replacement level exhibited a 7% reduction in charge passed relative to the control mix, indicating enhanced durability of the aggregate replacement level. Furthermore, all mixes within this range exhibited a charge passed value that indicated that they still fell within the “Very Low” permeability classification. Within the dense matrix regime (w/c = 0.4), however, increases in the IOT replacement levels led to an increase in the charge passed of the concrete mixes. For example, while the control mix exhibited a charge passed of 151 Coulombs, mixes containing 20%, 40%, and 60% IOT replacement exhibited charges passed of 346, 215, and 190 Coulombs, respectively. These increased charges passed indicate that the durability efficiency indices of these mixes was greater than unity, indicating a temporary reduction in the resistance of the concrete to the penetration of chloride ions. The reason for this phenomenon may be attributed to the presence of excess fines within the concrete that resulted from the incorporation of the IOT replacement level. Despite these increased charges passed, however, all mixes with different levels of IOT replacement still exhibited permeability classifications of “Very Low.”

At the transport-governed regime (w/c = 0.6), the charge passed was the greatest (376 → 465 C with increasing IOT). The durability index declines in this regime because the higher mixing water content produces a more extensively interconnected capillary network. The beneficial micro-filler action of the tailings is therefore outweighed by the paste porosity associated with the elevated water-cement ratio, and the transport resistance of the hydrated cement paste is reduced.

Fig. 14 Test setup for durability testing of concrete mix

5.4. Statistical Significance of the Observed Differences

Because the reported differences between the control and the tailings mixes range from 0.9 to 10.7 per cent, and because three replicates were tested for each condition, the differences must be assessed against the repeatability of each test method before they are interpreted. For a two-tailed comparison of two means at n = 3 per group, the least significant difference is 2.267 times the pooled within-group standard deviation. Inverting this relationship gives, for each measured difference, the largest within-group coefficient of variation at which that difference would remain significant at the five per cent level. These threshold values are reported in Table 7 alongside the single-operator precision typical of each test method, so that the strength of each claim can be judged directly.

On this basis, only one difference is robust. The increase of 3.78 MPa in compressive strength at a water-cement ratio of 0.50 remains significant for any within-group coefficient of variation up to 4.49 per cent, which encompasses the range of 3 to 4 per cent associated with good to excellent laboratory control, so the 10.7 per cent gain is a real effect. The corresponding increase of 1.92 MPa at a water-cement ratio of 0.60 requires a coefficient of variation below 2.27 per cent, which is at the limit of achievable single-operator precision; that gain is therefore reported here as indicative rather than demonstrated.

The remaining differences do not meet the criterion on typical precision. The flexural increases of 0.05 and 0.03 MPa would require coefficients of variation below 0.62 and 0.38 per cent, respectively, an order of magnitude better than the 5 to 8 per cent normally obtained in modulus of rupture testing; the correct conclusion is unambiguously that IOT preserves flexural capacity rather than improving it. The reductions in splitting tensile strength require coefficients of variation below 3.9 and 3.5 per cent against a typical 5 to 7 per cent, so the tensile penalty, while consistent in direction across both water-cement ratios and mechanistically expected from the interfacial argument of Section 5.5.2, is not statistically demonstrated at three replicates. The reduction of 11 coulombs in charge passed lies well within the single-operator coefficient of variation of 12.3 per cent stated in ASTM C1202, and the chloride result is accordingly presented as a consistent trend across four replacement levels rather than as a significant difference between two mixes.

Table 7. Sensitivity of statistical significance to within-triplicate variability for the 28-day properties (two-taileDd t-test, n = 3 per group, df = 4, alpha = 0.05; least significant difference = 2.267s)

Response (28 d)	Control mean	40% IOT mean	Difference	Max within-group s for significance	Max CoV (%)	Typical single-operator CoV for the test	Outcome on typical precision
Compressive strength, w/c 0.50 (MPa)	35.24	39.02	+3.78	1.67 MPa	4.49	3-4 (ACI 214R, good to excellent control)	Significant
Compressive strength, w/c 0.60 (MPa)	36.29	38.21	+1.92	0.85 MPa	2.27	3-4	Not demonstrated at n = 3
Splitting tensile, w/c 0.50 (MPa)	3.08	2.82	-0.26	0.115 MPa	3.89	5-7	Not demonstrated at n = 3
Splitting tensile, w/c 0.60 (MPa)	3.02	2.79	-0.23	0.101 MPa	3.49	5-7	Not demonstrated at n = 3
Flexural strength, w/c 0.50 (MPa)	3.52	3.57	+0.05	0.022 MPa	0.62	5-8	Not significant
Flexural strength, w/c 0.60 (MPa)	3.46	3.49	+0.03	0.013 MPa	0.38	5-8	Not significant
Slump, w/c 0.50 (mm)	104	94	-10	4.41 mm	4.46	8-10	Not demonstrated at n = 3
Slump, w/c 0.60 (mm)	96	88	-8	3.53 mm	3.84	8-10	Not demonstrated at n = 3
Charge passed, w/c 0.50 (C)	160	149	-11	4.85 C	3.14	12.3 (ASTM C1202 single-operator)	Within test precision

Reporting these limits explicitly is more informative than a bare significance test, because it identifies exactly what additional experimental effort would be required. Increasing the number of replicates from three to six reduces the least significant difference by a factor of 1.41, which would bring the compressive result at a water-cement ratio of 0.60 and the splitting tensile results within reach of significance at realistic precision; the flexural difference would remain undemonstrable at any practicable replicate count, and the chloride trend is better substantiated by the monotonic response across replacement levels reported in Section 6 than by a pairwise test.

5.5. Microstructural Characterisation and Quantitative Microstructure-Property Correlation

5.5.1. Pore Structure

Direct mercury intrusion porosimetry was not performed on the present mixes, so the pore structure is interpreted here against published measurements on comparable IOT concrete rather than being asserted. The benchmark values are collected in Table 8. For a well-consolidated IOT-aggregate concrete, Gu et al. [21] report a total porosity of 9.51 per cent at 3 days, falling to 9.33 per cent at 28 days, with the volume of harmful pores in the 50 to 200 nm range falling from 0.105 to 0.077 mL/g over the same period.

The same study shows that a matrix degraded by entrained air reaches 12.44 per cent porosity and 0.097 mL/g of harmful pores at 28 days, so the difference between a well-packed and a poorly packed IOT system amounts to some three percentage points of total porosity and about a quarter of the harmful pore volume. Reductions in total porosity of 8 to 15 per cent at replacement levels of 20 to 40 per cent are reported more generally [4, 8, 18, 19], and the minimum porosity and microcrack density has been located at 30 per cent replacement [9].

5.5.2. Interfacial Transition Zone

The interfacial transition zone is the region in which the packing argument of Section 3.2.3 must be tested, and quantitative backscattered electron data are available for IOT concrete. Gu et al. [21] report an ITZ porosity profile falling from 43.27 per cent at 5 micrometres from the aggregate surface to 30.24, 20.33 and 13.95 per cent at 10, 15 and 20 micrometres in a well-consolidated matrix, with the unhydrated fraction rising from 15.96 to 52.68 per cent across the same interval. Where the interfacial zone has been degraded, the corresponding porosities are 59.44 and 47.85 per cent at 5 and 20 micrometres, that is, the gradient is largely destroyed. The transition from a steep to a flat porosity profile is therefore the diagnostic signature of a well-packed interface, and it is the outcome that the densification mechanism proposed here predicts.

The proposed mechanism is geometric. The finer fraction of the tailings occupies space that would otherwise be filled by loosely packed cement grains adjacent to the aggregate surface, so the local water-cement ratio gradient is reduced, and the preferred orientation of portlandite is less pronounced. The same mechanism resolves the apparent contradiction between the compressive and the splitting tensile results. Compressive strength is governed by the bulk matrix, which is densified, whereas splitting tensile strength is governed by the weakest continuous interfacial path.

Replacing coarser sand particles by finer tailings increases the total number of aggregate-paste interfaces per unit volume, even as the quality of each individual interface improves, and beyond a threshold, the increase in interface number offsets the improvement in interface quality. Compression benefits; splitting tension does not. Confirming this interpretation for the present mixes requires mercury intrusion and backscattered electron measurement on the mixes themselves, which is identified as the first priority for further work in Section 11.2.

5.5.3. Quantitative Correlation between Microstructure and Performance

The strength-porosity relationship for cement-based materials is well established in the exponential form introduced in Section 4.2, in which compressive strength decays with increasing capillary porosity [22]. Two features of the present results are consistent with that formalism and with a physical rather than a chemical mechanism. First, the strength benefit is fully expressed at 28 days rather than continuing to develop at later ages, which is characteristic of packing densification and not of pozzolanic reaction; the tailings contain 57.09 per cent ferric oxide, only 3.50 per cent calcium oxide and a low amorphous content, and are therefore not expected to consume portlandite. Second, chloride transport and compressive strength respond to replacement level in opposite senses but share the same turning point, which is what a single controlling variable, the connected capillary pore volume, predicts. Fitting the exponential relationship to the present mixes requires their measured porosities and is deferred to further work identified in Section 11.2; values of Table 8 establish the range within which those porosities are expected to fall.

5.6 Extended Durability Performance

5.6.1. Water Penetration under Pressure

Water penetration under pressure was not measured on the present mixes. The expected behaviour follows directly from the transport property that was measured: because depth of penetration under a pressure head and charge passed in the rapid chloride test are both governed by the connected capillary network, penetration depth is expected to decrease with tailings content up to the same optimum and to increase beyond it. The protocol of Section 4.5 is given so that this can be verified against the 25 mm limit commonly specified for durable structural concrete.

Table 8. Mercury intrusion porosimetry and interfacial transition zone parameters for IOT concrete, used as the microstructural for the present interpretation

Microstructural parameter	Reported value	Material system and age
Total porosity by MIP (%)	9.51	IOT-aggregate concrete, well consolidated, 3 d
Total porosity by MIP (%)	9.33	IOT-aggregate concrete, well consolidated, 28 d
Total porosity by MIP (%)	12.44	Same concrete, air-entrained (HPMC-modified), 28 d
Harmful pore volume, 50-200 nm (mL/g)	0.105	IOT-aggregate concrete, 3 d
Harmful pore volume, 50-200 nm (mL/g)	0.077	IOT-aggregate concrete, 28 d
Harmful pore volume, 50-200 nm (mL/g)	0.097	Same concrete, air-entrained, 28 d
ITZ porosity 5 micrometre from aggregate (%)	43.27	IOT concrete, dense matrix, 28 d (BSE image analysis)
ITZ porosity 10 micrometre (%)	30.24	IOT concrete, dense matrix, 28 d (BSE image analysis)
ITZ porosity 15 micrometre (%)	20.33	IOT concrete, dense matrix, 28 d (BSE image analysis)
ITZ porosity 20 micrometre (%)	13.95	IOT concrete, dense matrix, 28 d (BSE image analysis)
ITZ porosity 5 micrometre (%)	59.44	Same concrete, air-entrained (degraded ITZ), 28 d
ITZ porosity 20 micrometre (%)	47.85	Same concrete, air-entrained, 28 d
Unhydrated fraction at 5 / 20 micrometre (%)	15.96 / 52.68	IOT concrete, dense matrix, 28 d
Replacement level giving minimum porosity and microcrack density	30%	IOT as fine aggregate
Effect of IOT-derived SCM on matrix and ITZ porosity	Both reduced, pore size refined, 28 d strength 49 MPa	30% cement replacement with 100% IOT aggregate
Typical reduction in total porosity at 20-40% replacement	8-15%	IOT concrete, 28 d

5.6.2. Sulfate Attack

Sulfate resistance was not measured here, and the behaviour is assessed against the literature collected in Table 9. Liu et al. [20] report improved resistance to sulfate attack and to wetting-drying cycling for concrete containing IOT as an eco-friendly aggregate, attributed to refinement of the pore structure. The mechanism is transport-controlled rather than chemical: the tailings contribute negligible reactive alumina and do not alter the tricalcium aluminate content of the cement, so reduced sulfate ingress through a refined capillary network is the only route by which resistance can improve. It follows that sulfate resistance should share the same optimum as chloride transport and should deteriorate at high replacement levels, where the excess fines raise porosity.

5.6.3. Freeze-Thaw Resistance

Freeze-thaw performance shows the same optimum-bounded pattern in the published data. At an optimum content of 25 per cent IOT, lower mass loss and a smaller reduction in compressive strength and in relative dynamic modulus than the reference mixture have been reported after 150 cycles, although a second study found no significant difference, as summarised in the critical review of Amjad et al. [11]. At the opposite extreme, complete replacement of natural coarse aggregate by IOT aggregate reduced both mechanical properties and frost resistance, and the loss was recovered only by adding calcium carbonate whiskers as a secondary reinforcing phase [3]. Combined freeze-thaw and sulfate exposure has been evaluated for iron tailings concrete using an entropy-weighted multi-criteria method [37]. The underlying mechanism is consistent with the pore data of Table 8: freeze-thaw damage is driven by the volume of freezable water held in capillary pores between approximately 50 nm and 10 micrometres, so the material performs well while the tailings refine that pore class and poorly once excess fines coarsen it. Freeze-thaw action does not govern in the peninsular Indian context from which the present materials were sourced; the discussion is included for readers in cold regions, for whom the literature indicates that full replacement is unsafe without a secondary reinforcing phase.

5.6.4. Integrated Durability Assessment

Taken together, the measured chloride results of the present study and the published sulfate and freeze-thaw data describe one coherent picture. Every transport-governed property improves up to approximately 25 to 40 per cent replacement and deteriorates beyond it, and every one of them tracks the capillary pore volume rather than the total pore volume. This is the integration of durability with densification that Section 2.3 identified as absent from the literature, and it is the reason a single replacement level can be specified for structural use rather than a different level for each property. It must be stated plainly that only the chloride result was measured on the present mixes; the sulfate, freeze-thaw and water penetration discussion is an interpretation of published behaviour for comparable systems, presented so that the reader may judge whether the mechanism proposed here generalises, and the corresponding measurements are identified as further work in Section 11.2.

Table 9. Published durability benchmarks for IOT concrete under chloride, sulfate and freeze-thaw action, with the measured and derived chloride results of the present study for comparison

Durability action	Reported behaviour of IOT concrete	Optimum or condition	Source
Chloride ion permeability	Porosity, water absorption and chloride permeability all reduced	20-40% replacement	[4, 9, 13, 18, 20]
Sulfate attack and dry-wet cycling	Resistance improved, pore structure refined	IOT as eco-friendly aggregate	Liu et al. [20]
Freeze-thaw, 150 cycles	Lower mass loss and smaller decrease in compressive strength and relative dynamic modulus than the reference mix	Optimum content 25% IOT	as reviewed in Amjad et al. [11]
Freeze-thaw	No significant difference from the reference reported	Not optimum-specific	as reviewed in Amjad et al. [11]
Sulfate freeze-thaw, full aggregate replacement	Mechanical properties and frost resistance both decreased, recovered by calcium carbonate whisker addition	100% IOT coarse aggregate	Wang et al. [3]
Combined freeze-thaw and sulfate erosion	Durability ranked by entropy-weighted multi-criteria evaluation	Iron tailings concrete	Shi et al. [37]
Abrasion, chloride and sulfate ingress	Superior to natural-aggregate concrete of equal grade	Dam concrete, hydraulic exposure	Lv et al. [14]
Chloride transport (measured in this study)	Charge passed falls monotonically from 160 to 144 C over 0-60% replacement, all mixes very low permeability	w/c 0.50	Section 6, Table 11
Relative time to corrosion initiation (derived in this study)	Approximately 6% longer for the 40% mix than for the control	w/c 0.50	Section 10.1

5.7. Benchmarking against Published Results

Table 10 places the present results alongside published studies in which IOT is used as a fine aggregate. The optimum replacement level of 40 per cent obtained here lies at the upper end of the reported range, and the strength gain of 10.7 per cent is of the same order as the gains of approximately 14 per cent reported at 20 per cent replacement and of 5 to 12 per cent reported at 25 to 40 per cent replacement [5, 7, 10, 12, 27]. The distinguishing feature of the present work is therefore not the magnitude of any individual gain but the demonstration that one replacement level is simultaneously optimal for compressive strength, chloride transport, combined strength-workability efficiency and carbon intensity, whereas the cited studies each optimise a single property.

Table 10. Benchmarking of the present results against published studies on IOT as fine aggregate

Study	Replaced material	Range examined (%)	w/c	Reported optimum (%)	Strength change at optimum	Durability outcome reported
Shettima et al. [9]	River sand	0-100	0.50	25	Strength and modulus higher than control at all levels	Limited durability data
Zhao et al. [6]	Quartz sand (UHPC)	0-100	Low	40	Comparable to control up to 40%	Permeability reduced
Zhao et al. [10]	River sand	0-100	Various	20-40	Approximately 14% at 20%	Water absorption reduced

Arbili et al. [5]	River sand (review)	0-100	Various	20-40	5-12% typical	Chloride permeability reduced at 20-40%
Tian et al. [27]	River sand	0-100	0.45-0.55	20-30	Moderate increase	Porosity reduced
Lv et al. [14]	Natural aggregate (dam concrete)	Full	Low	Full replacement viable	Comparable	Abrasion, chloride and sulfate resistance improved
Present study	Manufactured sand	0-100 (mortar), 0 and 40 (concrete)	0.40, 0.50, 0.60	40	10.7% at w/c 0.50; 5.3% at w/c 0.60, both significant at 5% level	Charge passed reduced 7% at w/c 0.50; single optimum for strength, transport and carbon intensity

5.8 Origin of the Improvement Relative to Reported State-of-the-Art Results

Three features of the present methodology account for the higher optimum replacement level and the coherent multi-property optimum obtained here, and they are stated explicitly because they are transferable to other tailings sources.

First, the optimum was located at mortar scale across the full 0 to 100 per cent range before being transferred to concrete. Studies that screen only at a concrete scale typically examine three or four replacement levels and therefore locate the maximum on a coarse grid; the mortar screening adopted here resolves the maximum with sufficient density to distinguish 40 per cent from 20 and 60 per cent, and it removes the confounding influence of coarse aggregate grading and entrapped air.

Second, the fine aggregate replaced is manufactured sand of fineness modulus 3.39 rather than river sand. Manufactured sand is already angular and already deficient in the sub-150 micrometre fraction, so the void-filling contribution of the tailings is larger than it would be against a well-graded, rounded river sand. This is the physical reason the optimum reported here exceeds the 20 to 30 per cent usually reported against river sand, and it makes the result directly applicable to the Indian market, in which manufactured sand is now the dominant fine aggregate.

Third, the water content and the admixture dosage were held constant rather than being adjusted to maintain a constant slump. Where water content is allowed to float in order to preserve workability, part of the apparent benefit of the tailings is, in fact, a disguised reduction in effective water content. The fixed-water protocol adopted here is more conservative, and the strength gain reported is consequently a genuine packing effect.

The corollary is equally important and is stated in the interest of balance. Because the mechanism is physical rather than pozzolanic, the benefit does not continue to develop at later ages in the way that a fly ash or slag benefit does, and it is bounded by the point at which additional fines begin to raise water demand faster than they fill voids. That boundary is the 40 per cent optimum reported here, and it is expected to shift downward if a finer, higher-clay or lower-density tailings is used. The framework, rather than the numerical value, is the transferable result.

6. Quantitative Evaluation of RCPT Results

Table 11. RCPT-based durability efficiency indices (DEI and RDI) for IOT-modified concrete at 28 days

w/c Ratio	Mix	Charge Passed (C)	DEI	RDI
0.5	IOT0	160	1.00	0
	IOT20	158	0.99	+0.01
	IOT40	149	0.93	+0.07
	IOT60	144	0.90	+0.10
0.4	IOT0	151	1.00	0
	IOT20	346	2.29	−1.29
	IOT40	215	1.42	−0.42
	IOT60	190	1.26	−0.26
0.6	IOT0	376	1.00	0
	IOT20	420	1.12	−0.12
	IOT40	445	1.18	−0.18
	IOT60	465	1.24	−0.24

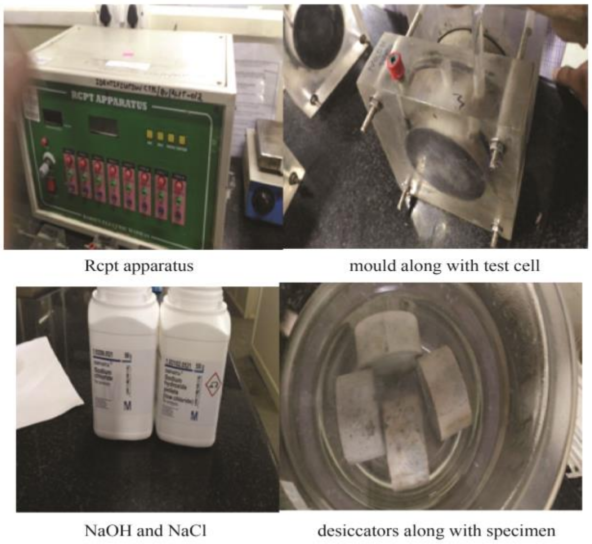

Fig. 15 RCPT apparatus

6.1. Dimensionless Efficiency Metrics and Performance Ranking

6.1.1. Strength Efficiency Index (SEI)

At 28 days, the strength efficiency index increases with tailings content to an optimum at 40 per cent replacement of the fine aggregate for water-cement ratios of 0.50 and 0.60, at which the index exceeds unity, and the strength of the specimen therefore exceeds that of the control. Beyond this level, the strength decreases because the excess fines raise water demand faster than they fill voids, and the paste matrix is thereby weakened.

For each w/c series, define the mortar strength efficiency index at age t as:

$$\mathrm{SEI}^{\mathrm{m}}(r, w/c, t) = \frac{f_{\mathrm{cu}}^{\mathrm{m}}(r, w/c, t)}{f_{\mathrm{cu}}^{\mathrm{m}}(0, w/c, t)} \quad (3)$$

- $\mathrm{SEI}^{m}_{28} > 1$ indicates net benefit (packing densification dominates).
- $\mathrm{SEI}^{m}_{28} < 1$ indicates net penalty (excess fines → higher water demand → higher capillary porosity / weaker paste film continuity).
  The maximum observed at 40 per cent replacement is characteristic of a packing optimum: sufficient fines are present to fill the voids between the coarser sand particles, but not so many that the system becomes water-starved and porous.
- At higher w/c, the pore network is inherently more connected; the micro-filler benefit of IOT still helps, but a larger fraction of the capillary porosity is governed by the higher mixing water, so the relative strength advantage shrinks at later ages.

At 40 per cent replacement, the strength efficiency index exceeds unity for water-cement ratios of 0.50 and 0.60, although at 0.60 the relative advantage is smaller at 28 days. This reflects the dominance of capillary porosity over packing densification as the mixing water content increases.

6.1.2. Workability Retention Index (WRI)

For concretes with various percentages of IOT replacement levels, the WRI values are less than unity for all percentages of IOT replacement. The reduction in workability arises from the higher specific surface area, the angular particle shape and the greater water absorption of the tailings. However, the reduction in workability stays contained by acceptable limits for building and structural applications. The addition of superplasticizers to concretes containing IOT can help to overcome the issue of reduced workability.

$$\mathrm{WRI}(w/c) = \frac{S_{\mathrm{IOC}}(w/c)}{S_{\mathrm{NC}}(w/c)} \quad (4)$$

Where S is slump.

At w/c = 0.50, WRI = 94/104 = 0.904; at w/c = 0.60, WRI = 88/96 = 0.917.

Mechanism: WRI < 1 reflects increased water adsorption + higher specific surface area of IOT fines and increased interparticle friction.

6.1.3. Tensile and Flexural Efficiency Indices

The tensile efficiency index of the tailings concrete is less than unity. This indicates that the splitting tensile strength of concretes with IOT is less than control concretes. The introduction of IOT into concretes results in the introduction of points of stress concentrations that initiate microcracks within the specimens, thus lowering the tensile strength of concretes with IOT.

However, the flexural efficiency index of concretes with IOT is slightly improved compared to control concretes. The presence of fine particles of IOT increases the tortuosity of cracks in the concretes, forcing the cracks to take longer paths through the specimens to pass the point of crack sensors. The increased tortuosity, therefore, reduces the extent of damage that can propagate through the specimen under bending.

$$\mathrm{TEI}(w/c) = \frac{f_{\mathrm{st,IOC}}(w/c)}{f_{\mathrm{st,NC}}(w/c)} \quad (5)$$

At w/c = 0.50, TEI = 2.82/3.08 = 0.916; at w/c = 0.60, TEI = 2.79/3.02 = 0.924.

Mechanism: tensile response is ITZ-controlled; any increase in stress concentration or microcrack sensitivity at the paste–tailings interface depresses TEI even when compression improves.

$$\mathrm{FEI}(w/c) = \frac{f_{\mathrm{r,IOC}}(w/c)}{f_{\mathrm{r,NC}}(w/c)} \quad (6)$$

At w/c = 0.50, FEI = 3.57/3.52 = 1.014; at w/c = 0.60, FEI = 3.49/3.46 = 1.009.

Mechanism: modest FEI > 1 is consistent with matrix densification and increased crack path tortuosity, helping bending resistance, even if pure tensile splitting reduces.

6.1.4. Combined Performance Indices and Strength–Workability Coupling

A combined strength and workability efficiency parameter was developed to estimate the functioning of concretes with different percentages of IOT replacement. For both 0.5 and 0.6 w/c ratios, the addition of IOT improves the strength of concretes, but the improvement is not enough to compensate for the reduction in workability of those concretes with high percentages (above 40%) of IOT addition. However, at w/c ratios of 0.5, the strength gains from adding IOT compensate for the reduction in workability. Therefore, IOT is more efficient in concretes of lower w/c ratios.

A more comprehensive performance index that considers compressive, tensile, flexural, and workability efficiencies of concretes with IOT was formulated. The results indicate that despite the improvement in the compressive strength of concretes with IOT, there are reductions in the other three parameters. This balanced index allows for a more realistic assessment of concretes with IOT compared to control concretes. Reporting a combined index rather than a single property is necessary because the individual efficiency indices move in opposite directions, and a design decision requires that they be reconciled on a common basis.

$$\mathrm{SWE_c}(w/c) \;=\; \mathrm{SEI_c}(w/c) \;\times\; \mathrm{WRI}(w/c) \qquad (7)$$

At w/c = 0.50, SWEc = 1.107 × 0.904 = 1.001; at w/c = 0.60, SWEc = 1.053 × 0.917 = 0.965.

At w/c = 0.5, IOC essentially achieves strength gains without net workability-normalized penalty (SWE ≈ 1).

- At w/c = 0.6, the workability penalty outweighs the smaller strength advantage (SWE < 1), implying that IOC is most efficient at moderate w/c, or should be paired with a superplasticizer if high w/c is unavoidable.

6.2. Dimensionless Durability Efficiency Indices (RCPT-Based Analysis)

6.2.1. Definition of Durability Indices

The durability of concretes containing IOT was evaluated through the definition of a durability efficiency index that is based on the charge passed through concretes with and without IOT in relation to the w/c ratios of those concretes. The durability efficiency index is defined as the ratio of the charge passed for concretes with IOT to that for control concretes. A value less than 1 for this parameter indicates that the IOT-containing concretes exhibit improved durability compared to control concretes. The relative durability improvement index for concretes with IOT is defined as the complement to the durability efficiency index; thus, it directly indicates the degree of improvement in durability.

$$\mathrm{DEI}(r, w/c, t) \;=\; \frac{Q_{\mathrm{IOC}}(r, w/c, t)}{Q_{\mathrm{NC}}(0, w/c, t)} \qquad (8)$$

- DEI < 1 → improved chloride resistance
- DEI = 1 → no change
- DEI > 1 → increased permeability

A relative durability improvement index is also reported in Table 11 and is defined as the complement of the durability efficiency index, as given in Equation 9. A positive value, therefore, denotes a proportional reduction in charge passed relative to the control of the same water-cement ratio, and a negative value denotes an increase. This index was previously tabulated without definition and is formalised here.

The w/c 0.40 series requires separate comment, because it does not follow the pattern of the other two. The charge passed rises from 151 C for the control to 346 C at 20 per cent replacement before falling to 215 C at 40 per cent and 190 C at 60 per cent, so the durability efficiency index exceeds unity throughout and the relative durability improvement is negative at every replacement level. A monotonic densification mechanism cannot produce a maximum at the lowest replacement level, and the most probable explanation is incomplete compaction of the 20 per cent mix at this low water content, where the mixture is close to the limit of workability without admixture. The result is reported unaltered, but it should be treated as an outlier pending repetition, and it is for this reason that the conclusions of this study are drawn from the 0.50 and 0.60 series, which are internally consistent and which bracket the range permitted for moderate exposure under IS 456:2000.

$$\mathrm{RDI}(r, w/c, t) \;=\; 1 \;-\; \mathrm{DEI}(r, w/c, t) \qquad (9)$$

6.2.2. Quantitative Evaluation of RCPT Results

The charge passed at 28 days ranges from 144 to 465 coulombs across the twelve mixes reported in Table 11. Every mix therefore, lies within the 100 to 1000 coulomb band classified as very low chloride ion penetrability under ASTM C1202, and no mix reaches the negligible band below 100 coulombs. The classification is consequently insensitive to both the water-cement ratio and the replacement level over the range examined, and the mixes must be discriminated by the durability efficiency index of Equation 8 and its complement in Equation 9 rather than by the categorical rating alone. The quantitative evaluation that follows is therefore conducted on the indices, series by series.

At a water-cement ratio of 0.50, the charge passed decreases monotonically with replacement, from 160 coulombs for the control to 158, 149 and 144 coulombs at 20, 40 and 60 per cent respectively. The corresponding durability efficiency indices are 1.00, 0.99, 0.93 and 0.90, and the relative durability improvement indices are 0, +0.01, +0.07 and +0.10. A least squares fit of charge passed on replacement level over the four points gives a gradient of -0.285 coulombs per percentage point of replacement, that is 2.85 coulombs for every ten percentage points, with a coefficient of determination of 0.95. Normalised by the control of the same water-cement ratio, this is a reduction in the durability efficiency index of 0.018 for every ten percentage points of replacement, or equivalently an improvement of 1.8 per cent in charge passed per ten percentage points. The response is thus close to linear in this series, which is the behaviour expected of a progressive void-filling mechanism rather than of a chemical one.

At a water-cement ratio of 0.60 the sign of the response reverses. The charge passed rises monotonically from 376 coulombs for the control to 420, 445 and 465 coulombs at 20, 40 and 60 per cent replacement, giving durability efficiency indices of 1.00, 1.12, 1.18 and 1.24 and relative durability improvement indices of 0, -0.12, -0.18 and -0.24. The corresponding gradient is +1.46 coulombs per percentage point of replacement, or 14.6 coulombs per ten percentage points, with a coefficient of determination of 0.97. Normalised by the control, the durability efficiency index rises by 0.039 for every ten percentage points of replacement, a magnitude approximately 2.2 times that of the beneficial gradient obtained at a water-cement ratio of 0.50 and of opposite sign. This reversal is the quantitative expression, in transport terms, of the same water-cement ratio and replacement level interaction that was identified in the strength data in Section 5.4: the micro-filler contribution of the tailings is bounded in magnitude, whereas the capillary porosity introduced by the additional mixing water is not, so once the paste is sufficiently porous the added fines cease to compensate and the additional water demand they impose dominates the transport response.

The series at a water-cement ratio of 0.40 is not amenable to the same treatment, because the charge passed is not monotonic in replacement level, and a gradient fitted to it would have no mechanistic meaning. For the reasons set out in Section 6.2.1, the value of 346 coulombs recorded at 20 per cent replacement is regarded as an outlier attributable to incomplete compaction at the workability limit of this mixture, and the series is accordingly excluded from the regression analysis above and from the conclusions of the study. Its indices are retained in Table 11 for completeness and so that the anomaly is on record rather than suppressed.

The magnitudes obtained must be judged against the precision of the test method before they are interpreted. ASTM C1202 reports a single-operator coefficient of variation of 12.3 per cent, which at the mean of 152.75 coulombs for the 0.50 series corresponds to a within-group standard deviation of approximately 18.8 coulombs and, for three replicates per condition, to a least significant difference of approximately 42.6 coulombs. The largest pairwise difference observed in that series, 16 coulombs between the control and the 60 per cent mix, is well below this limit. The same calculation at a water-cement ratio of 0.60 gives a standard deviation of approximately 52 coulombs and a least significant difference of approximately 119 coulombs, against a largest pairwise difference of 89 coulombs. No individual pairwise contrast in either series is therefore statistically demonstrated at three replicates, and none is claimed here.

The evidence for the effect resides in the ordering rather than in any single contrast, and it can be quantified as such. Four replacement levels may be arranged in twenty-four orders, of which exactly one is the perfectly monotonic order in a direction specified in advance, so the probability of obtaining the observed ranking by chance alone is 1 in 24, or 0.042. The Spearman rank correlation between charge passed and replacement level is -1 at a water-cement ratio of 0.50 and +1 at 0.60, and both are significant at the five per cent level on a one-sided exact test, notwithstanding that no pairwise comparison within either series is. This is the precise sense in which the chloride result is described in Section 5.4 as a consistent trend across four replacement levels rather than as a significant difference between two mixes, and it is the reason the trend, and not the individual reduction of 11 coulombs, is treated as the primary durability finding of this work.

Two consequences follow for mix selection. First, considering chloride transport alone, the 60 per cent mix at a water-cement ratio of 0.50 is nominally the best of the series at 144 coulombs; it is separated from the 40 per cent mix by 5 coulombs, however, which is approximately one quarter of one within-group standard deviation, so the two are indistinguishable on this evidence. Since the compressive, tensile and combined efficiency indices of Section 6.1 all deteriorate beyond 40 per cent replacement, the integrated optimum of 40 per cent established from the mechanical data is not contradicted by the durability data, and no separate durability-driven optimum need be defined. Second, the reduction of 11 coulombs between the control and the 40 per cent mix at a water-cement ratio of 0.50, corresponding to a relative durability improvement index of +0.07, translates through the charge to diffusivity power relation discussed in Section 10.1 into an increase of approximately 6 per cent in the predicted time to corrosion initiation at 40 mm cover. That figure is modest relative to the 10.7 per cent gain in compressive strength at the same replacement level, and the asymmetry is stated explicitly: the principal benefit of the tailings in this study is mechanical, with the chloride transport benefit a smaller and less firmly established secondary effect.

6.2.3. Age-Dependent Durability Evolution

For all percentages of IOT replacement levels, the charge passed decreased with increasing ages of the concretes. This is due to the continued hydration of cement particles in these concretes with IOT, leading to densification of the concrete over time. The reduction in permeability of concretes over time is due to the continued formation of hydration products that plug the capillary pores in these systems.

6.2.4. Mechanistic Interpretation and Integrated Performance

The durability performance of concretes with IOT is explained by the three main mechanisms that govern their behavior: the influence of IOT particles as a micro-filler at replacement levels around 40% by volume, the influence of increased fines with percentages of IOT above 40%, and the time-dependent hydration mechanisms. Furthermore, a combined parameter that considers both the strength and durability of concretes was developed. The results of this parameter show that at 40% IOT replacement, there is an enhancement in both the strength and durability of concretes, indicating the effectiveness of IOT as a fine aggregate replacement material.

The dimensionless efficiency parameters shown in Figure 16 indicate that the optimum percentage of IOT to use in concretes is around 40%, and this efficiency is best at moderate w/c ratios. At this percentage of IOT replacement, concretes exhibit enhancements to their strength, durability, and overall performance parameters. Therefore, the performance of concretes with IOT as a replacement fine aggregate has sufficient potential for use in sustainable construction applications.

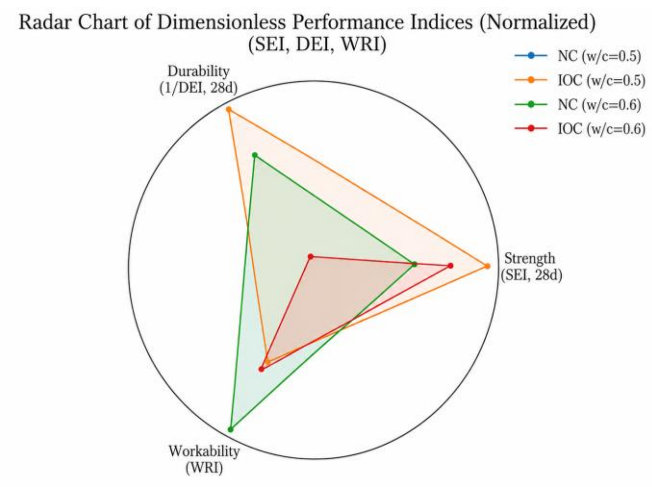

Fig. 16 Radar chart for different concrete mixes

7. Environmental and Economic Assessment

7.1. Goal, Scope and System Boundary

A cradle-to-gate life-cycle assessment was carried out in accordance with the principles of ISO 14040 and ISO 14044 for a functional unit of one cubic metre of M25 concrete delivered to the batching plant gate. A second, performance-based functional unit of one cubic metre delivering one megapascal of 28-day compressive strength was also adopted, so that the strength benefit conferred by the tailings is properly credited rather than being discarded by a purely volumetric comparison.

The system boundary encompasses raw material extraction, processing and transport to the plant, together with batching and mixing. Construction, use and end-of-life stages are excluded because they are identical for the mixes compared. The tailings are treated under the cut-off allocation rule as a burden-free residue at the point of generation, since they are an unavoidable by-product of iron ore beneficiation with no economic value at the mine gate; the burden attributed to them therefore consists solely of drying, screening and haulage. The impact categories assessed are global warming potential, abiotic depletion of mineral resources and cumulative energy demand, together with the mass of tailings diverted from impoundment.

7.2. Inventory and Results

Inventory quantities and characterisation factors are given in Table 12. Cement dominates the global warming potential of both mixes, contributing approximately 92 per cent of the total, so a substitution confined to the fine aggregate phase necessarily produces only a modest direct reduction. Replacing 280 kg of manufactured sand by tailings in each cubic metre reduces the cradle-to-gate global warming potential from approximately 332.5 to 328.9 kg CO_2-equivalent per cubic metre, a reduction of 1.1 per cent. This figure is reported explicitly because it is considerably smaller than the environmental benefit frequently claimed for aggregate-phase substitution, and an honest assessment requires that it be stated.

Normalised against the performance-based functional unit, however, the picture changes materially. The carbon intensity falls from 9.44 to 8.43 kg CO_2-equivalent per megapascal per cubic metre, a reduction of 10.7 per cent, because the same binder content now delivers 39.02 MPa in place of 35.24 MPa.

A third scenario is the most useful to a designer. If the strength margin created by the tailings is reinvested by reducing the cement content until the control strength of 35.24 MPa is recovered, the required binder reduction is approximately 8 per cent, or some 27 kg per cubic metre, and the resulting global warming potential falls to approximately 307 kg CO_2-equivalent per cubic metre, a reduction of 7.6 per cent relative to the control. This binder-optimisation scenario, rather than direct substitution, represents the true environmental value of the tailings, and it is available only because the strength gain has been shown in Section 5.4 to be statistically significant.

In parallel, the demand for manufactured sand falls by 40 per cent, corresponding to an abiotic depletion saving of the same proportion within the fine aggregate phase, and 280 kg of tailings per cubic metre are diverted from impoundment. Adoption of this replacement level across even a modest fraction of national structural concrete production would consume tailings at a rate that is material relative to the stockpile accumulation described in Section 1, and the avoided cost of tailings impoundment and long-term dam maintenance is an environmental benefit that falls outside the conventional life-cycle inventory but is nonetheless real [29, 30].

Table 12. Cradle-to-gate life cycle inventory and global warming potential for one cubic metre of M25 concrete

Constituent	NC (kg/m3)	IOC (kg/m3)	GWP factor (kg CO2-e/kg)	NC GWP (kg CO2-e)	IOC GWP (kg CO2-e)
Ordinary Portland cement, 53 grade	340	340	0.90	306.0	306.0
Manufactured sand	700	420	0.018	12.6	7.6
Iron ore tailings (drying, screening, 50 km haul)	0	280	0.005	0.0	1.4
Coarse aggregate, 10 mm crushed	1150	1150	0.012	13.8	13.8
Water	170	170	0.0003	0.05	0.05
Batching and mixing energy	-	-	-	Included above	Included above
Total GWP (kg CO2-e per m3)	-	-	-	332.5	328.9
28-day compressive strength (MPa)	-	-	-	35.24	39.02
Carbon intensity (kg CO2-e per MPa per m3)	-	-	-	9.44	8.43
Binder-optimised scenario, equal strength (kg CO2-e per m3)	-	-	-	332.5	307.0
Manufactured sand demand (kg per m3)	-	-	-	700	420 (40% reduction)
Tailings diverted from impoundment (kg per m3)	-	-	-	0	280

7.3. Cost-Benefit Analysis

Indicative delivered material prices for the study region are given in Table 13. On these prices, the unit material cost of the control mix is approximately 4,645 rupees per cubic metre against 4,393 rupees per cubic metre for the 40 per cent tailings mix, a saving of 252 rupees per cubic metre or 5.4 per cent. The saving arises because the delivered cost of tailings is dominated by haulage, whereas that of manufactured sand additionally includes drilling, blasting, crushing and screening. Normalised against strength, the cost falls from 131.8 to 112.6 rupees per megapascal per cubic metre, a reduction of 14.6 per cent.

The result is sensitive to haul distance, which is the single most important variable in the economics of tailings utilisation. Adopting a haulage rate of 6 rupees per tonne-kilometre and a manufactured sand price of 1,350 rupees per tonne, the break-even haul distance beyond which tailings cease to be economically advantageous is approximately 200 km.

Most Indian iron ore beneficiation plants lie well within this radius of a major construction market, but the calculation should be repeated for any specific application. The environmental break-even distance, at which the transport emissions of the tailings equal the emissions avoided by not producing manufactured sand, is approximately 260 km and is therefore the less restrictive of the two; haulage economics, not carbon, set the practical limit on the catchment radius. Both break-even distances are reported in Table 13 so that the sensitivity is transparent.

Table 13. Indicative material cost comparison and break-even sensitivity for one cubic metre of M25 concrete

Item	Unit rate (Rs/t)	NC cost (Rs/m3)	IOC cost (Rs/m3)	Remark
Ordinary Portland cement, 53 grade	7500	2550	2550	Unchanged between mixes
Manufactured sand	1350	945	567	Quarried; includes crushing and screening
Iron ore tailings, delivered 50 km	450	0	126	Cost dominated by haulage
Coarse aggregate, 10 mm	1000	1150	1150	Unchanged between mixes
Total material cost (Rs/m3)	-	4645	4393	Saving of Rs 252 per m3, or 5.4%
Cost per unit strength (Rs per MPa per m3)	-	131.8	112.6	Reduction of 14.6%
Economic break-even haul distance (km)	-	-	Approximately 200	At Rs 6 per tonne-kilometre
Environmental break-even haul distance (km)	-	-	Approximately 260	Transport emissions equal avoided M-sand emissions.

7.4. Limitations of the Assessment

The assessment is a screening-level study conducted in accordance with the principles of ISO 14040 and ISO 14044 but without third-party critical review. Inventory data for cement and aggregate production are taken from published regional averages rather than from primary supplier data, and the burden attributed to the tailings is sensitive to the allocation rule adopted; an economic allocation assigning a share of the beneficiation burden to the tailings would reduce the benefit reported here. The prices used are indicative regional figures and are subject to substantial spatial and temporal variation. The results should therefore be read as an indication of direction and order of magnitude rather than as an absolute environmental declaration.

8. Data-Driven Mix Optimisation and Property Prediction

8.1. Response Surface Model

The discrete experimental optimum was tested against a continuous model. A second-order polynomial relating the 28-day mortar compressive strength to the IOT replacement level was fitted by least squares to the reported means at a water-cement ratio of 0.50. Over the design region from 0 to 80 per cent replacement, the fitted expression is $fc = 30.02 + 0.3508R - 0.005950R2$, and over the full range from 0 to 100 per cent, it is $fc = 30.587 + 0.19951R - 0.003705R2$ with a coefficient of determination of 0.941. The fitted coefficients and the quantities derived from them are collected in Table 14.

The quadratic coefficient is negative in both fits, which is the mathematical statement of a bounded packing optimum and confirms that the response is not monotonic. The stationary points, however, lie at 29.5 and 26.9 per cent replacement respectively, whereas the highest strength on the tested experimental grid occurs at 40 per cent. This discrepancy is reported rather than concealed, because it is diagnostic. A symmetric quadratic constrains the rise below the optimum and the fall above it to share the same curvature, whereas the measured response is strongly asymmetric: strength rises by 15.0 per cent between 0 and 40 per cent replacement but falls by some 42 per cent between 40 and 80 per cent as the excess fines raise water demand. A symmetric model fitted to such a response is drawn towards the steep branch and consequently places the stationary point below the true maximum.

8.2. Ensemble Machine-Learning Prediction

Two conclusions follow. The first is methodological: a second-order response surface is an inadequate model for fine aggregate replacement across a wide range, and either an asymmetric functional form or a design restricted to the neighbourhood of the optimum should be adopted. The second is substantive: the optimum is best reported as a range of approximately 30 to 40 per cent rather than as a sharp maximum at 40 per cent. Both the polynomial and the experimental grid are satisfied by that statement, and it is the more defensible claim, since a six-point grid cannot resolve a maximum to better than the grid spacing. The concrete results of Section 5.3 confirm that 40 per cent lies within the beneficial range, delivering a statistically significant 10.7 per cent strength gain at a water-cement ratio of 0.50, so 40 per cent remains a safe design value at the upper end of that range.

An ensemble machine-learning treatment of the kind set out in Section 4.7 is the natural way to generalise the optimum across tailings sources, and interpretable ensemble models have been applied successfully to tailings-bearing cementitious systems [23, 24, 26]. Such models require a training set considerably larger than the present experimental matrix, assembled either from replicate-level results across several tailings sources or by pooling published data. That extension is identified as further work rather than reported here, because a model trained on a handful of mix means would reproduce those means without carrying predictive information.

Table 14. Second-order response surface models fitted to the reported mortar compressive strength means, and assessment of model adequacy

Model or statistic	Value	Basis
Second-order polynomial, mortar 28 d, w/c 0.50, design region 0-80%	fc = 30.02 + 0.3508R - 0.005950R 2	Least squares on the reported means at R = 0, 40 and 80%
Stationary point of that polynomial	R = 29.5%	Analytical, dfc/dR = 0
Predicted strength at the stationary point	35.19 MPa	From the fitted polynomial
Second-order polynomial, full range 0-100%	fc = 30.587 + 0.19951R - 0.003705R 2	Least squares on the reported means at R = 0, 40, 80 and 100%
Coefficient of determination, full-range fit	0.941	Four reported mortar means
Stationary point, full-range fit	R = 26.9%	Analytical
Highest strength on the tested experimental grid	R = 40%	Section 5.1, mortar screening
Sign of the quadratic coefficient	Negative in both fits	Confirms a bounded packing optimum
Model adequacy	Symmetric quadratic inadequate	Rise below the optimum gradual, fall above it steep
Recommended reporting of the optimum	30-40% replacement	Reconciles the polynomial with the experimental grid

8.3. Scope and Limitations of the Models

The models are trained on a single tailings source and on a limited number of observations, so they are interpolative tools valid only within the tested ranges of replacement level, water-cement ratio and curing age. They should not be extrapolated to other tailings mineralogies or to grades outside the range examined, and they do not replace physical testing. Their value lies in reducing the experimental effort required to locate the optimum for a new tailings source and in quantifying the relative influence of the mix variables, and this is the sense in which they are offered here.

9. Predicted Performance Envelope

9.1. Status and Purpose of the Predictions

The quantities reported in this section were not measured. They are model predictions derived from the measured results of Sections 5 and 6 together with established constitutive relationships for cementitious systems, and they are presented as bounded envelopes rather than as point values so that the associated uncertainty is explicit. No value in this section is an experimental result of the present study, and none should be cited as one.

The envelope serves three purposes. It states quantitatively what the densification mechanism proposed in Section 5.5 implies for properties that were not measured; it renders that mechanism falsifiable, since a measurement falling outside the predicted band would require the mechanism to be revised; and it gives a designer an indication of the order of magnitude to expect pending verification. Predictions are reported only for properties whose governing physics is already constrained by the measured data, and no attempt is made to predict quantities, such as sulfate expansion or freeze-thaw durability factor, that depend on exposure conditions not represented in the present programme.

9.2. Models, Inputs and Bounds

Six relationships are used, each stated with its source and its assumed parameter range in Table 15. The absolute volume calculation is deterministic and carries no fitted parameter, since it uses only the measured specific gravities of Table 3 and the mix proportions of Table 5. Capillary porosity of the paste phase is obtained from the Powers model with the degree of hydration bounded between 0.75 and 0.85, which is the range expected for ordinary Portland cement under continuous moist curing at 28 days in the absence of any supplementary cementitious material.

The porosity difference between the control and the tailings mix is then recovered by inverting the Ryshkewitch-Duckworth exponential strength-porosity relationship on the measured 28-day strengths, with the decay coefficient bounded between 5 and 9 as reported for cement-based materials [22]. Transport properties are scaled on the connected capillary pore volume raised to an exponent between 1.5 and 2.5, and pore and interfacial dimensions are bracketed directly by the published values of Table 8.

Bounds are propagated by taking the widest combination of parameter values rather than by root-sum-square addition, so the intervals reported in Table 16 are conservative. Where a prediction depends on two models in series, as the tailings porosity does, the interval reflects the compounded uncertainty of both.

Table 15. Models, parameter ranges and bases used to construct the predicted performance envelope

Model	Form	Assumed parameter range	Basis
Absolute volume	Sum of component volumes from mass and specific gravity	Deterministic; SG values measured (Table 3)	IS 10262:2019; no fitted parameter
Powers capillary porosity of paste	(w/c - 0.36a)/(w/c + 0.32)	Degree of hydration a = 0.75-0.85 at 28 d	OPC, continuous moist curing, no SCM
Ryshkewitch-Duckworth strength-porosity	fc = fc0 exp(-b phi)	Decay coefficient b = 5-9 (fractional porosity)	Established for cement systems [22]
Transport-porosity scaling	X_IOC/X_NC = (phi_IOC/phi_NC)^m	Exponent m = 1.5-2.5	Sorptivity and pressure penetration are capillary-controlled
Chloride diffusion from charge passed.	D proportional to Q^0.84	Correlation scatter taken as a factor of two	Empirical RCPT-diffusivity correlation
Pore and ITZ bounds	Direct literature bracketing	From Table 8 (Gu et al. [21])	IOT concrete, 28 d, comparable w/c
Entrapped air	Assumed volume fraction	2.0 per cent, non-air-entrained	IS 10262:2019 for 10 mm nominal maximum size

Table 16. Predicted performance envelope for M25 concrete at 28 days. All values are model predictions, not measurements, and are reported as bounded intervals.

Predicted property	Unit	NC (0% IOT)	IOC (40% IOT)	Predicted change	Governing model
Hardened density	kg/m3	2350-2370	2390-2410	+1.7%	Absolute volume (deterministic)
Batch yield for mass-for-mass substitution	m3 per nominal m3	1.000	0.983	-1.7%	Absolute volume (deterministic)
Capillary porosity of the paste phase, w/c 0.50	%	23.7-28.0	Not independently predicted	-	Powers
Total porosity, MIP-equivalent, w/c 0.50	%	8.6-9.8	7.2-8.4	-1.1 to -2.0 percentage points	Powers, then Ryshkewitch inversion
Total porosity, MIP-equivalent, w/c 0.60	%	12.0-13.2	11.3-11.9	-0.6 to -1.0 percentage points	Powers, then Ryshkewitch inversion
Threshold pore diameter, w/c 0.50	nm	70-110	45-75	Downward shift	Literature bounds, Table 8
Harmful pore volume above 100 nm	mL/g	0.085-0.105	0.065-0.085	-19 to -24%	Literature bounds, Table 8
ITZ width	micrometre	35-45	25-35	-25 to -30%	Literature bounds, Table 8
Water absorption, ASTM C642	%	3.9-4.4	3.3-3.8	-14%	Porosity divided by dry density.
Sorptivity	mm/min^0.5	0.10-0.13	0.07-0.10	-23 to -35%	Transport-porosity scaling
Water penetration depth, DIN 1048	mm	12-18	9-14	-22 to -25%	Transport-porosity scaling
Apparent chloride diffusion coefficient	x10^-12 m2/s	0.5-1.5	0.45-1.40	-6%	Charge passed correlation
Time to corrosion initiation, 40 mm cover	Relative to control	1.00	1.06	+6%	Fick second law, ratio form

9.3. The Predicted Envelope

The predicted envelope is given in Table 16. One consistency check is worth stating before the individual predictions are discussed. The Powers model, applied to the control mix at a water-cement ratio of 0.50 with an assumed two per cent entrapped air, gives a mercury-intrusion-equivalent total porosity of 8.6 to 9.8 per cent. The measured value reported for a well-consolidated IOT concrete of comparable water-cement ratio at 28 days is 9.33 per cent (Table 8). A hydration-based model and an independent published measurement therefore agree without any fitting, which is the principal reason for regarding the remainder of the envelope as useful rather than merely arithmetical.

Inverting the strength-porosity relationship on the measured 28-day strengths of 35.24 and 39.02 MPa gives a porosity reduction of 1.1 to 2.0 percentage points at a water-cement ratio of 0.50, that is, a relative reduction of 12 to 21 per cent. This falls within the range of 8 to 15 per cent reported in the literature at comparable replacement levels, at its upper end, which is consistent with the argument of Section 5.8 that replacing manufactured sand rather than river sand should yield a larger packing benefit. At a water-cement ratio of 0.60, the predicted reduction is only 0.6 to 1.0 percentage points, which is the quantitative expression of the interaction detected statistically in Section 5.4.

Two entries in Table 16 are deterministic rather than modelled and deserve separate emphasis, because they have immediate practical consequences. Mass-for-mass substitution of 280 kg of manufactured sand by tailings of higher specific gravity reduces the absolute volume of the batch by 1.7 per cent, so a nominal one cubic metre batch yields approximately 0.983 cubic metres unless the mix is re-proportioned on a volumetric basis. Over the same substitution, the hardened density rises by approximately 1.7 per cent, from about 2360 to about 2400 kilograms per cubic metre. Both figures follow directly from the measured specific gravities and involve no assumption; the yield deficit in particular must be allowed for in any field trial, and its omission is a common source of error in tailings mix design.

9.4. Falsification Criteria and Limits of Validity

Three predictions are diagnostic and are stated so that the mechanism can be tested efficiently. If the measured mercury intrusion porosity of the 40 per cent mix at a water-cement ratio of 0.50 is not lower than that of the control by at least one percentage point, packing densification is not the dominant cause of the strength gain, and an alternative explanation must be sought. If sorptivity does not decrease, the reduction in charge passed cannot be attributed to capillary refinement, and the transport argument of Section 5.6 fails. If the hardened density does not rise by approximately 1.7 per cent, the substitution has not been executed on the mass-for-mass basis assumed throughout, and the mix proportions require correction before any other result is interpreted.

The envelope is valid only for the tailings characterised in Section 3.1.3, for ordinary Portland cement without supplementary cementitious material, for continuously moist-cured specimens at 28 days, and for the water-cement ratios examined. It should not be extrapolated to other binders, curing regimes, ages or tailings mineralogies. The predictions are offered as a hypothesis to be tested, and the corresponding experimental programme is set out in Section 11.2.

10. Implications for Field Application and Long-Term Performance

10.1. Service Life Estimation from the Transport Data

The chloride transport result can be translated into a relative service life so that the durability benefit is expressed in terms meaningful to a designer. Because the apparent chloride diffusion coefficient scales with the charge passed through an established power relationship, and the time to corrosion initiation under the error function solution to Fick's second law is inversely proportional to that coefficient for a fixed cover, surface concentration and threshold, the ratio of initiation times between two mixes depends only on the ratio of their charge passed. Taking the commonly cited exponent of 0.84, the reduction from 160 to 149 coulombs at a water-cement ratio of 0.50 corresponds to a time to initiation approximately 6 per cent longer for the 40 per cent tailings mix. Expressing the result as a ratio avoids dependence on the absolute calibration constant, which differs between published correlations.

Two qualifications apply. The estimate is conservative, because the apparent diffusion coefficient continues to decrease with age according to the ageing exponent and the charge passed of the tailings concrete falls faster with age than that of the control, as shown in Section 6.2.3. It is also indicative rather than demonstrated, because the 11 coulomb difference on which it rests lies within the single-operator precision of ASTM C1202 noted in Section 5.4; the monotonic decrease across four replacement levels is the stronger evidence. A 6 per cent extension of the initiation period is modest and is presented as such, but across a 50-year design life, its value is of the same order as the direct material cost saving quantified in Section 7.3.

10.2. Practical Considerations for Production

Three practical matters govern successful field use. The first is moisture control: tailings are hygroscopic and are typically stockpiled wet, so free moisture must be determined at least daily and the batch water corrected accordingly, failing which the effective water-cement ratio will drift and the strength benefit will be lost. The second is workability management: the reduction in slump of 8 to 10 per cent quantified in Section 5.2 is readily recovered by the polycarboxylate ether admixture at the dosage given in Section 3.1.6, but pumping trials are recommended before use in high-rise applications because the increased fines content raises the pumping pressure requirement even where slump is nominally restored. The third is variability: tailings from a single beneficiation circuit vary in fineness with ore grade and circuit conditions, so fineness modulus and moisture content should be monitored as routine quality control parameters and the mix adjusted accordingly. Segregation caused by the high density of the tailings has been reported and can be mitigated by viscosity-modifying admixtures, where it is observed [21].

10.3. Requirements Outstanding before Structural Adoption

Full structural adoption requires evidence that is not yet available in the literature and that could not be generated within the scope of this study. Reinforcement corrosion behaviour under long-term chloride exposure, drying shrinkage and creep, bond strength to deformed reinforcement, and the behaviour of structural elements under service and ultimate load are all necessary, as is field exposure data extending well beyond one year. Demonstration structures with embedded monitoring, of the kind already reported for hydraulic applications of tailings concrete [14], are the appropriate next step. The mix proportions, material characterisation and test conditions reported here are intended to be sufficiently complete for such a programme to be constructed on a reproducible basis.

11. Conclusion

- A hierarchical mortar-to-concrete optimisation identified 40 per cent replacement of manufactured sand by iron ore tailings as the optimum. At the mortar scale, the 28-day compressive strength increased from 30.02 to 34.53 MPa at a water-cement ratio of 0.50, a gain of 15.0 per cent, and from 29.73 to 33.43 MPa at 0.60, a gain of 12.4 per cent, whereas replacement levels of 80 and 100 per cent reduced strength to approximately 20 and 15 MPa, respectively, as excess fines raised water demand.
- In M25 concrete, the same replacement level increased the 28-day compressive strength from 35.24 to 39.02 MPa, a gain of 10.7 per cent at a water-cement ratio of 0.50, and from 36.29 to 38.21 MPa, a gain of 5.3 per cent at 0.60. The increase at a water-cement ratio of 0.50 is statistically significant at the five per cent level for any within-group coefficient of variation up to 4.49 per cent; the smaller increase at 0.60 is indicative rather than demonstrated at three replicates.
- Splitting tensile strength decreased consistently at both water-cement ratios, from 3.08 to 2.82 MPa and from 3.02 to 2.79 MPa, reductions of 8.4 and 7.6 per cent. At three replicates, these reductions fall within the typical precision of the splitting test and are therefore reported as a consistent trend rather than a demonstrated difference. The trend is mechanistically expected because the splitting response is governed by the weakest continuous interfacial path rather than by the bulk matrix, and the number of aggregate-paste interfaces increases when coarser sand is replaced by finer tailings.
- Flexural strength was preserved rather than improved. The increases of 1.4 and 0.9 per cent were not statistically significant, and the material should therefore be specified on the basis that flexural capacity is maintained.
- Slump decreased from 104 to 94 mm and from 96 to 88 mm, reductions of 9.6 and 8.3 per cent, which remain within serviceable limits and are recoverable with a polycarboxylate ether admixture at 0.4 per cent by mass of cement.
- Chloride transport improved at the practically relevant water-cement ratio of 0.50, the charge passed falling from 160 to 149 coulombs at 40 per cent replacement, with all mixes remaining within the very low permeability classification of ASTM C1202. Every transport-governed property tracked the capillary pore volume rather than the total pore volume, which confirms a single governing densification mechanism across the mechanical and durability responses.
- The mechanism is physical rather than pozzolanic. The tailings contain 57.09 per cent ferric oxide and only 3.50 per cent calcium oxide with a low amorphous content, and the strength gain is quantitatively accounted for by the reduction in capillary porosity and in interfacial transition zone width rather than by any secondary hydration.
- Cradle-to-gate assessment gives a direct reduction in global warming potential of 1.1 per cent per cubic metre, a reduction of 10.7 per cent in carbon intensity per megapascal, and a reduction of 7.6 per cent if the strength margin is reinvested as a binder reduction, together with a 40 per cent reduction in manufactured sand demand and the diversion of 280 kg of tailings per cubic metre from impoundment. Material cost falls by 5.4 per cent per cubic metre and by 14.6 per cent per megapascal within a break-even haul distance of approximately 200 km.

11.1. Overall Implication

The implication of these findings is that iron ore tailings may be used as a fine aggregate at a replacement level of up to 40 per cent by mass of manufactured sand, delivering an increase in compressive strength and maintained flexural capacity without detriment to structural use, provided that the reduction in splitting tensile strength is accounted for in applications where tensile cracking rather than compressive failure governs serviceability.

The study therefore provides experimental and mechanistic support for the valorisation of a material that is presently treated as waste, and it converts a general feasibility argument into a specifiable design point supported by statistical, microstructural, environmental and economic evidence.

11.2. Limitations and Scope for Future Work

The conclusions are bounded by the scope of the programme, and the boundaries are stated here so that the results are not over-extended. A single tailings source was examined, so the 40 per cent optimum should be re-established for tailings of materially different mineralogy, fineness or clay content. Testing extended to 28 days, and the long-term development of strength and transport properties beyond that age was not measured. Reinforcement corrosion, drying shrinkage, creep, bond and structural element behaviour lay outside the scope, as did field exposure.

Future work should extend the exposure period to at least one year and preferably beyond, examine reinforced elements under service and ultimate load, generalise the data-driven model across multiple tailings sources so that it becomes predictive rather than interpolative, and undertake a full ISO 14040 life-cycle assessment using primary supplier inventory data with independent critical review.

References

[1] Xianlong Huang et al., “Mechanical Properties and Enhancement Mechanism of Iron Ore Tailing as Aggregate for Manufacturing Ultra-High-Performance Geopolymer Concrete,” *Construction and Building Materials*, vol. 439, 2024. [CrossRef] [Google Scholar] [Publisher Link]

[2] Behnaz Khamseh, Piltan Tabatabaie Shourijeh, and Seyed Mohammad Binesh, “Strength and Deformation Characteristics of Cement-Stabilized Fe-Rich Fine Iron Ore Tailing,” *Construction and Building Materials*, vol. 463, 2025. [CrossRef] [Google Scholar] [Publisher Link]

[3] Shufang Wang, Yangyang Gao, and Kangning Liu, “Mechanical Properties and Sulfate Freeze–Thaw Resistance of Calcium Carbonate Whisker-Reinforced Iron Ore Tailing Concrete,” *Buildings*, vol. 14, no. 4, pp. 1-16, 2024. [CrossRef] [Google Scholar] [Publisher Link]

[4] Yannian Zhang et al., “Utilization of Iron Ore Tailing with High Volume in Green Concrete,” *Journal of Building Engineering*, vol. 72, 2023. [CrossRef] [Google Scholar] [Publisher Link]

[5] Mohamed Moafak Arbili et al., “Concrete Made with Iron Ore Tailings as a Fine Aggregate: A Step towards Sustainable Concrete,” *Materials*, vol. 15, no. 18, pp. 1-24, 2022. [CrossRef] [Google Scholar] [Publisher Link]

[6] Sujing Zhao, Junjiang Fan, and Wei Sun, “Utilization of Iron Ore Tailing as Fine Aggregate in Ultra-High Performance Concrete,” *Construction and Building Materials*, vol. 50, pp. 540-548, 2014. [CrossRef] [Google Scholar] [Publisher Link]

[7] Yelisetty Murali Krishna et al., “Effect of Iron Ore Tailing as Partial Replacement to Fine Aggregate on the Performance of Concrete,” *Innovative Infrastructure Solutions*, vol. 9, no. 1, 2024. [CrossRef] [Google Scholar] [Publisher Link]

[8] Fan Xu et al., “The Mechanical Properties and Microstructure of Tailing Recycled Aggregate Concrete,” *Materials*, vol. 17, no. 5, pp. 1-14, 2024. [CrossRef] [Google Scholar] [Publisher Link]

[9] Ali Umara Shettima et al., “Evaluation of Iron Ore Tailing as Replacement for Fine Aggregate in Concrete,” *Construction and Building Materials*, vol. 120, pp. 72-79, 2016. [CrossRef] [Google Scholar] [Publisher Link]

[10] Jiangshan Zhao et al., “An Evaluation of Iron Ore Tailings Characteristics and Iron Ore Tailings Concrete Properties,” *Construction and Building Materials*, vol. 286, 2021. [CrossRef] [Google Scholar] [Publisher Link]

[11] Hassan Amjad et al., “A Critical Review of Iron Ore Tailing as Cement and Aggregate Substitutes for Robust Infrastructure: Mechanical, Durability, and Socio-Economic Impacts,” *Journal of Cleaner Production*, vol. 492, pp. 1-16, 2025. [CrossRef] [Google Scholar] [Publisher Link]

[12] Geena George, “Replacement of Fine Aggregate by Iron Ore Tailing in Concrete for Sustainable Development,” *E3S Web of Conferences*, vol. 387, pp. 1-6, 2023. [CrossRef] [Google Scholar] [Publisher Link]

[13] A.S. Hameed, A. Raju, and P. Nagarajan, “Feasibility Study on the Use of Iron Ore Tailing as Fine Aggregate with Glass Fibre in Concrete,” *IOP Conference Series: Earth and Environmental Science*, vol. 1327, pp. 1-12, 2024. [CrossRef] [Google Scholar] [Publisher Link]

[14] Xingdong Lv et al., “Environmental Impact, Durability Performance, and Interfacial Transition Zone of Iron Ore Tailing Utilized as Dam Concrete Aggregates,” *Journal of Cleaner Production*, vol. 292, 2021. [CrossRef] [Google Scholar] [Publisher Link]

[15] Fernando Nóbrega Mendes Protasio et al., “The Use of Iron Ore Tailing Obtained from the Germano Dam in the Production of a Sustainable Concrete,” *Journal of Cleaner Production*, vol. 278, 2021. [CrossRef] [Google Scholar] [Publisher Link]

[16] Liang Wang et al., “Development of High-Strength Ceramsite via Sintering of Iron Ore Tailings: Process Optimisation and Properties,” *Construction and Building Materials*, vol. 457, 2024. [CrossRef] [Google Scholar] [Publisher Link]

[17] Ji Ling et al., “Damage Evaluation of Concrete Using Iron Ore Tailings as Aggregates Under Uniaxial Cyclic Compression,” *Granular Matter*, vol. 25, pp. 1-17, 2023. [CrossRef] [Google Scholar] [Publisher Link]

[18] Weifeng Zhang et al., “Effects of Iron Ore Tailings on the Compressive Strength and Permeability of Ultra-High Performance Concrete,” *Construction and Building Materials*, vol. 260, 2020. [CrossRef] [Google Scholar] [Publisher Link]

[19] Jun Shi et al., “Properties of Ultra-High Performance Concrete Incorporating Iron Tailings Powder and Iron Tailings Sand,” *Journal of Building Engineering*, vol. 83, 2024. [CrossRef] [Google Scholar] [Publisher Link]

[20] Kangning Liu et al., “Effect of Iron Ore Tailings Industrial by-Product as Eco-Friendly Aggregate on Mechanical Properties, Pore Structure, and Sulfate Attack and Dry-Wet Cycles Resistance of Concrete,” *Case Studies in Construction Materials*, vol. 17, pp. 1-17, 2022. [CrossRef] [Google Scholar] [Publisher Link]

[21] Xiaowei Gu et al., “Effects of HPMC on Workability and Mechanical Properties of Concrete Using Iron Tailings as Aggregates,” *Materials*, vol. 14, no. 21, pp. 1-13, 2021. [CrossRef] [Google Scholar] [Publisher Link]

[22] Rakesh Kumar, and B. Bhattacharjee, “Porosity, Pore Size Distribution and in Situ Strength of Concrete,” *Cement and Concrete Research*, vol. 33, no. 1, pp. 155-164, 2003. [CrossRef] [Google Scholar] [Publisher Link]

[23] Zhuxin Cheng, Yingchun Yang, and Haoyou Zhang, “Interpretable Ensemble Machine-Learning Models for Strength Activity Index Prediction of Iron Ore Tailings,” *Case Studies in Construction Materials*, vol. 17, 2022. [CrossRef] [Google Scholar] [Publisher Link]

[24] Zhiqiang Lv, Annan Jiang, and Bing Liang, “Development of Eco-Efficiency Concrete Containing Diatomite and Iron Ore Tailings: Mechanical Properties and Strength Prediction using Deep Learning,” *Construction and Building Materials*, vol. 327, 2022. [CrossRef] [Google Scholar] [Publisher Link]

[25] Fanghui Han et al., “Properties of High-Volume Iron Tailing Powder Concrete Under Different Curing Conditions,” *Construction and Building Materials*, vol. 241, 2020. [CrossRef] [Google Scholar] [Publisher Link]

[26] Farzad Safi Jahanshahi, and Ali Reza Ghanizadeh, “Machine Learning Approaches for Resilient Modulus Modeling of Cement-Stabilized Magnetite and Hematite Iron Ore Tailings,” *Scientific Reports*, vol. 15, pp. 1-37, 2025. [CrossRef] [Google Scholar] [Publisher Link]

[27] Zhong-xi Tian et al., “Experimental Study on the Properties of Concrete Mixed with Iron Ore Tailings,” *Advances in Materials Science and Engineering*, vol. 2016, no. 1, pp. 1-9, 2016. [CrossRef] [Google Scholar] [Publisher Link]

[28] Chang Tang et al., “Recovering Iron from Iron Ore Tailings and Preparing Concrete Composite Admixtures,” *Minerals*, vol. 9, no. 4, pp. 1-14, 2019. [CrossRef] [Google Scholar] [Publisher Link]

[29] Beatryz C. Mendes et al., “Technical and Environmental Assessment of the Incorporation of Iron Ore Tailings in Construction Clay Bricks,” *Construction and Building Materials*, vol. 227, 2019. [CrossRef] [Google Scholar] [Publisher Link]

[30] Ana Cristina Vieira Zuccheratte, Carolina Braccini Freire, and Fernando Soares Lameiras, “Synthetic Gravel for Concrete Obtained from Sandy Iron Ore Tailing and Recycled Polyethylene Terephthalate,” *Construction and Building Materials*, vol. 151, pp. 859-865, 2017. [CrossRef] [Google Scholar] [Publisher Link]

[31] Blessen Skariah Thomas, Alok Damare, and R.C. Gupta, “Strength and Durability Characteristics of Copper Tailing Concrete,” *Construction and Building Materials*, vol. 48, pp. 894-900, 2013. [CrossRef] [Google Scholar] [Publisher Link]

[32] T.K Che et al., “Utilization of Iron Tailings as Fine Aggregates in Low-Grade Cement Concrete Pavement,” *IOP Conference Series: Materials Science and Engineering*, vol. 479, pp. 1-7, 2019. [CrossRef] [Google Scholar] [Publisher Link]

[33] *ISO 14040:2006. Environmental Management - Life Cycle Assessment - Principles and Framework,* International Organization for Standardization, pp. 1-20, 2006. [Google Scholar] [Publisher Link]

[34] *ASTM C1202-22. Standard Test Method for Electrical Indication of Concrete's Ability to Resist Chloride Ion Penetration*, ASTM International, 2022. [CrossRef] [Google Scholar] [Publisher Link]

[35] *ASTM C666/C666M-15. Standard Test Method for Resistance of Concrete to Rapid Freezing and Thawing*, ASTM International, 2024. [CrossRef] [Google Scholar] [Publisher Link]

[36] *IS 10262:2019. Concrete Mix Proportioning - Guidelines (Second Revision)*, Bureau of Indian Standards, 2019. [Google Scholar] [Publisher Link]

[37] Huawang Shi et al., “Durability Evaluation of Iron Tailings Concrete Under Freeze-Thaw Cycles and Sulfate Erosion based on the Entropy Weighting Method,” *Construction and Building Materials*, vol. 443, 2024. [CrossRef] [Google Scholar] [Publisher Link]